ISSN 1674-1056
http://cpb.iphy.ac.cn
http://iopscience.iop.org/cpb
中国物理 B
Chinese Physics
中国物理
Chinese Physics B

Ultrasensitive nanosensors based on localized surface plasmon resonances: From theory to applications

Wen Chen(陈文), Huatian Hu(胡华天), Wei Jiang(姜巍), Yuhao Xu(徐宇浩), Shunping Zhang(张顺平), Hongxing Xu(徐红星)
Citation: Chin. Phys. B . 2018, 27(10): 107403. **doi:** 10.1088/1674-1056/27/10/107403

Journal homepage: http://cpb.iphy.ac.cn; http://iopscience.iop.org/cpb

What follows is a list of articles you may be interested in

Highly sensitive and stable SERS probes of alternately deposited Ag and Au layers on 3D SiO_2 nanogrids for detection of trace mercury ions

Yi Tian(田毅), Han-Fu Wang(王汉夫), Lan-Qin Yan(闫兰琴), Xian-Feng Zhang(张先锋), Attia Falak, Pei-Pei Chen(陈佩佩), Feng-Liang Dong(董凤良), Lian-Feng Sun(孙连峰), Wei-Guo Chu(褚卫国)
Chin. Phys. B . 2018, 27(7): 077406. **doi:** 10.1088/1674-1056/27/7/077406

The structure and elasticity of phase B silicates under high pressure by first principles simulation

Lei Liu(刘雷), Li Yi(易丽), Hong Liu(刘红), Ying Li(李营), Chun-Qiang Zhuang(庄春强), Long-Xing Yang(杨龙星), Gui-Ping Liu(刘桂平)
Chin. Phys. B . 2018, 27(4): 047402. **doi:** 10.1088/1674-1056/27/4/047402

High-pressure synchrotron x-ray diffraction and Raman spectroscopic study of plumbogummite

Duan Kang(康端), Xiang Wu(巫翔), Guan Yuan(袁冠), Sheng-Xuan Huang(黄圣轩), Jing-Jing Niu(牛菁菁), Jing Gao(高静), Shan Qin(秦善)
Chin. Phys. B . 2018, 27(1): 017402. **doi:** 10.1088/1674-1056/27/1/017402

Structural, elastic, and vibrational properties of phase H: A first-principles simulation

Chao-Jia Lv(吕超甲), Lei Liu(刘雷), Yang Gao(高阳), Hong Liu(刘红), Li Yi(易丽), Chun-Qiang Zhuang(庄春强), Ying Li(李营), Jian-Guo Du(杜建国)
Chin. Phys. B . 2017, 26(6): 067401. **doi:** 10.1088/1674-1056/26/6/067401

Quantitative analysis of ammonium salts in coking industrial liquid waste treatment process based on Raman spectroscopy

Ya-Nan Cao(曹亚南), Gui-Shi Wang(王贵师), Tu Tan(谈图), Ting-Dong Cai(蔡廷栋), Kun Liu(刘锟), Lei Wang(汪磊), Gong-Dong Zhu(朱公栋), Jiao-Xu Mei(梅教旭)
Chin. Phys. B . 2016, 25(10): 107403. **doi:** 10.1088/1674-1056/25/10/107403

TOPICAL REVIEW — Nanophotonics

Ultrasensitive nanosensors based on localized surface plasmon resonances: From theory to applications

Wen Chen(陈文)[1], Huatian Hu(胡华天)[2], Wei Jiang(姜巍)[1], Yuhao Xu(徐宇浩)[1], Shunping Zhang(张顺平)[1,†], and Hongxing Xu(徐红星)[1,2,‡]

[1] School of Physics and Technology, Center for Nanoscience and Nanotechnology, and Key Laboratory of Artificial Micro- and Nano-structures of Ministry of Education, Wuhan University, Wuhan 430072, China
[2] The Institute for Advanced Studies, Wuhan University, Wuhan 430072, China

(Received 5 July 2018; revised manuscript received 24 August 2018; published online 27 September 2018)

The subwavelength confinement feature of localized surface plasmon resonance (LSPR) allows plasmonic nanostructures to be functionalized as powerful platforms for detecting various molecular analytes as well as weak processes with nanoscale spatial resolution. One of the main goals of this field of research is to lower the absolute limit-of-detection (LOD) of LSPR-based sensors. This involves the improvement of (i) the figure-of-merit associated with structural parameters such as the size, shape and interparticle arrangement and, (ii) the spectral resolution. The latter involves advanced target identification and noise reduction techniques. By highlighting the strategies for improving the LOD, this review introduces the fundamental principles and recent progress of LSPR sensing based on different schemes including 1) refractometric sensing realized by observing target-induced refractive index changes, 2) plasmon rulers based on target-induced relative displacement of coupled plasmonic structures, 3) other relevant LSPR-based sensing schemes including chiral plasmonics, nanoparticle growth, and optomechanics. The ultimate LOD and the future trends of these LSPR-based sensing are also discussed.

Keywords: plasmonic sensing, localized surface plasmon resonance, plasmon rulers, nanoparticles

PACS: 74.25.nd,73.20.Mf,78.67.–n **DOI:** 10.1088/1674-1056/27/10/107403

1. Introduction

Metallic nanostructures can confine external optical field to a deep-subwavelength volume by virtue of localized surface plasmon resonance (LSPR), resulting in near-field enhancement of orders of magnitude with respect to the incident light. The field enhancement has been realized as the major contributor to the enhanced Raman signal of molecules in close vicinity to metallic nanostructures,[1] as early as in 1970s.[2,3] This phenomenon is known as surface-enhanced Raman scattering (SERS) and has been further developed over the years as a sensing scheme for fingerprint molecule detection with a sensitivity achieving single-molecule level.[4–6] Another important consequence of the localized plasmonic field is that the LSPR frequency is extremely sensitive to refractive index (RI) variations around the metallic nanostructures. This remarkable feature has been exploited for the development of refractometric sensing, which is capable of single-molecule detection[7–9] since the sensing volume is comparable to the size of a single analyte. The analyte-induced RI change within the local field can be conveniently converted to a discernable variation of a far-field physical parameter, such as wavelength, intensity, phase, or even the color observed by naked eye, without the need for the introduction of complicated near-field optics or electrical contacts. As a superior approach to other molecular sensing schemes with the analytes limited to either light-absorbable[10,11] or fluorescence (labeled)[12] species, LSPR-based sensors can realize real-time label-free probing of non-absorbing molecules, free from bleaching or blinking (which always occurs in fluorophores-labelled techniques) and disturbance of the analyte kinetics (which always occurs in SERS or molecule-labeled assay). Compared to commercial surface plasmon resonance (SPR) sensing using surface plasmon polaritons (SPP) on a metal film, LSPR sensing is at least one order of magnitude less sensitive to bulk changes in the RI, while exhibiting an improvement in the vertical spatial resolution by an order of magnitude.[13] As a result, this technique shows a similar sensitivity in the case of molecular sensing, where the analyte is attached to the metal surface.[14] Remarkably, LSPR sensors have a much higher lateral spatial resolution than SPR sensors (the former can reach single-nanoparticle level). These advantages suggest that LSPR sensors are well-suited to next-generation modern sensor architectures, because they can be compactly integrated into a microfluidic chip with simple optical configuration requirements, and can be inde-

*Project supported by the National Key Basic Research Program (Grant No. 2015CB932400), the National Key Research and Development Program of China (Grant Nos. 2017YFA0205800 and 2017YFA0303504), and the National Natural Science Foundation of China (Grant Nos. 11674255 and 11674256).

†Corresponding author. E-mail: spzhang@whu.edu.cn
‡Corresponding author. E-mail: hxxu@whu.edu.cn

© 2018 Chinese Physical Society and IOP Publishing Ltd

pendently operated.[13] They can function over a wide spectral range with great flexibility since the LSPR frequency depends on the size, shape, material type and arrangement of the nanostructure.

As a spectroscopic technique, the limit-of-detection (LOD) of LSPR sensing is defined as the smallest detectable signal output (spectral change) induced by analytes or detected events,[15] and is mainly determined by two characteristic performances: i) the spectral resolution limit and ii) the spectral change capability induced by the analytes or events. In the case of the refractometric sensing scheme, the latter can be characterized by a dimensionless figure-of-merits (FOM), defined as the ratio of the peak shift per unit RI change to the full width at half maximum (FWHM) of the LSPR peak.[16] Obtaining a higher FOM depends on several key factors. These include the controlled delivery of analytes to local 'hot spots' around the metal nanostructures and the use of dark plasmons[17–28] with less radiative damping, such as the Fano resonances and cavity plasmons, which have smaller FWHMs. The improvements in the designs for plasmonic sensing over the last two decades would not be feasible without significant advances in nanofabrication technologies. On one hand, complex electron- and ion-beam lithography techniques enable complicated patterning that can be matched in a straightforward manner to the requirements of multiplexed on-chip devices. On the other hand, wet chemical synthesis can facilitate the fabrication of inexpensive, naked eye colored metallic colloidal with different geometries. They can also be used to develop complex structures by applying self-assemble and chemical-linking techniques, thus allowing for the precise control of extremely small features extended to large area scaling.

Plasmonic nanostructures placed in close mutual proximity show pronounced collective LSPR, which is sensitive to the displacement of the gap distance. The discovery of metal dimer structures (Refs. [5] and [6]) with extremely strong electromagnetic field enhancement in the nanogap region between two nanoparticles offers the physical bases for such super sensitivity and many other interesting phenonmena in various strong coupled plasmonic structures. By utilizing this plasmon coupling phenomenon based on spectral recognition of changes in the interparticle distance, a displacement sensing scheme known as the plasmon ruler has been developed to monitor dynamic physical, chemical or biological processes. Importantly, the aforementioned advantages/features of the LSPR-active nanostructures are primarily inherited to this plasmon ruler assay. Currently, sensing concepts based on plasmonic response changes have been extended to a broad range of interdisciplinary field, *e.g.*, chiral sensing involving plasmonic fields[29] or self-assembly induced circular dichroism (CD) enhancements,[30,31] morphologic sensing schemes associated with nanoparticle growth[32] and active-plasmonic materials,[33] and plasmon nanomechanical transduction via the combination of a plasmon ruler scheme with a mechanical oscillator.[34] These tremendous developments broaden the boundaries of this research area to different degrees. Within this context, we will present an overview of the fundamental mechanism and current status of LSPR-based sensing associated with different transduction schemes, with an emphasis on the relevant strategies for improving sensing performance to achieve a sensitivity near the theoretical limit. In Section 2, the theoretical basis of the LSPR effect and its coupling theory will be introduced based on the plasmon hybridization model. In Section 3, recent progress in the LOD of LSPR sensing, including the FOM and spectral resolution will be discussed. In Section 4, we will describe the breakthrough of the displacement sensitivity of plasmon rulers and their typical applications. Finally, we will discuss the utilization of LSPR responses as other transduction schemes, including chiral sensing, nanoparticle growth, and optomechanics in Section 5.

2. Localized surface plasmon resonances in metal nanoparticles

In a simple Drude's scenario, the metal is treated as a free electron gas on a uniform background of positive charge. The performance of free electrons in the metal in response to an external electromagnetic field can be described by a frequency-dependent dielectric function $\varepsilon(\omega)$ according to the Drude model:[35]

$$\varepsilon(\omega) = 1 - \frac{\omega_{\mathrm{p}}^2}{\omega^2 + \mathrm{i}\gamma\omega}, \tag{1}$$

where ω is the angular frequency of the incident field and γ is the collision probability of free electrons. ω_{p} is the bulk plasma frequency of free electron oscillation, which is determined as

$$\omega_{\mathrm{p}} = \sqrt{\frac{Ne^2}{m\varepsilon_0}}, \tag{2}$$

where m is electron mass, e is the elementary charge, N is the density of the free electrons, and ε_0 is the permittivity of a vacuum. The Drude model only considers the contribution of free electrons in the conduction band while ignoring the effect of tightly-bounded electrons, *e.g.*, the inter-band transitions from the valence to the conduction band. In the high-frequency regime, Lorentz terms or a high-frequency component ε_∞ is always added for a more accurate fit of the performance of real metals. The real part of the dielectric function Re $[\varepsilon(\omega)]$ determines the resonance frequency of the oscillations of the electron, while the imaginary component Im $[\varepsilon(\omega)]$ represents the dephasing and damping of electron oscillations. The collision probability γ for a typical metal is about 100 THz–1000 THz,

which is much smaller than the frequency of visible and infrared light, namely, $\gamma \ll \omega$. In this case, the dielectric function of the metal mostly depends on the real part, thus equation (1) can be reduced as:

$$\varepsilon(\omega) = 1 - \frac{\omega_{\rm p}^2}{\omega^2}. \tag{3}$$

For a metallic structure with feature sizes down to nanoscale, its free electrons can be excited by an external electromagnetic field, thereby forming collective oscillations with the energy mostly confined to the surface. This phenomenon is known as LSPR, such that the localized polarization magnitude is described as $\boldsymbol{p} = \varepsilon_{\rm d}\alpha \boldsymbol{E}_0$, where $\varepsilon_{\rm d}$ is the permittivity of the dielectric material surrounding the nanoparticle, and α is the polarizability that determines the optical response of the electron gas in the nanoparticle. Thanks to the effort of Rayleigh, Mie, Gans, Napper, and Fuchs, the polarizabilities α of spherical and non-spherical nanoparticles, namely ellipsoids and cubes, are described by a general relation:[36]

$$\alpha = \varepsilon_0 V \sum_{i=1}^{N_i} C_i (1+\kappa_i) \frac{\varepsilon(\omega) - \varepsilon_{\rm d}}{\varepsilon(\omega) + \kappa_i \varepsilon_{\rm d}}, \tag{4}$$

where V is the volume of the nanoparticle, and C_i and κ_i are the oscillator strength and geometry factor due to the depolarization of the i-th mode. In the case where nanoparticles are excited by incident light whereby the effects of phase retardation (quasi-static approximation) is neglected, the oscillation of the electron gas can be approximately described by only the first order dipolar mode. The resonance condition of the LSPR is met when the polarizability α is a maximum, namely:

$$\mathrm{Re}\left[\varepsilon(\omega)\right] = -\kappa_1 \varepsilon_{\rm d}. \tag{5}$$

By plugging Eq. (5) into Eq. (3), $\omega_{\rm sp}$ can be expressed as:

$$\omega_{\rm sp} = \frac{\omega_{\rm p}}{\sqrt{1+\kappa_1 \varepsilon_{\rm d}}}. \tag{6}$$

Using the relation between the wavelength λ and angular frequency ω, along with the conversion from $\varepsilon_{\rm d}$ to refractive index n ($\varepsilon_{\rm d} = n^2$), $\omega_{\rm sp}$ can be converted to the LSPR wavelength $\lambda_{\rm sp}$, as:

$$\lambda_{\rm sp} = \lambda_{\rm p} \sqrt{1+\kappa_1 n^2}. \tag{7}$$

Thus, we can find that there is a linear relationship between the LSPR wavelength and the RI of the surrounding medium. Note that the linear dependence of the peak shift with respect to the RI is only satisfied in a small range of RI variation. On the other hand, the LSPR frequency depends on the material type (free electron density N). For instance, the LSPR wavelength of individual small Ag nanoparticles in air is approximately 380 nm. Although the free electron density between Ag and Au ($N_{\rm Ag} = 5.86 \times 10^{22}$ cm^{-3} and $N_{\rm Au} = 5.90 \times 10^{22}$ cm^{-3}) are similar, the LSPR wavelength of individual Au nanoparticles in air is damped to $\sim$ 520 nm with a significant broad peak width due to the presence of inter-band transitions from 3d to 4s band. In addition to these traditional metals, some nonmetal materials were also found to have pronounced plasmonic properties, including graphene[37–39] and doped semiconductor nanostructures.[40]

In terms of Eq. (7), the LSPR wavelength can also be strongly modified by the geometry of the plasmonic nanostructure. In several experiments, plasmonic nanoparticles with various shapes, such as sphere,[41,42] prism,[43] triangle,[44] cube,[16] shell,[45–47] rice,[48] star,[49] crescents,[50] rod,[51,52] bipyramid,[51,53] rattle,[54] *etc.*, have been synthesized by bottom-up wet chemical methods. On the other hand, methods based on top-down lithographic patterning have also been developed to create complex and periodic nanostructure extensions over a large area.[17,19,22,55,56] The advancement of these nanofabrication technologies lay the foundation for modifying the LSPR response via the fabrication of plasmonic materials with an arbitrary geometry. Actually, the LSPR wavelength also strongly relies on the size of the plasmonic nanoparticles. For particles with diameters that exceed 50 nm, the phase retardation effects start to play important roles, resulting in the redshift of the LSPR peak which is an almost linearly response to the particle size.[57]

3. LSPR-based refractometric sensing

3.1. Progress of figure-of-merit

According to Eq. (7), the LSPR-active nanostructures serve as an ideal refractometric sensing platform.[58] It relies on the observation of the LSPR spectral shift due to RI changes around the plasmonic surface induced by analyte binding events. The RI sensitivity S is defined as the amount of the peak shift per RI unit change (in units nm/RIU):

$$S = \frac{{\rm d}\lambda_{\rm sp}}{{\rm d}n}. \tag{8}$$

In practical applications, the LOD of the refractometric sensing is defined as the concentration of analyte derived from the smallest peak shift that can be recognized above the noise level, namely, the spectral contrast of the peak shift. This means that the LOD not only relates to the S, but also the FWHM of the LSPR peak. Generally, a larger nanoparticle exhibits a stronger and red-shifted LSPR peak, which leads to a higher S at the cost of an increased FWHM which lowers the spectral contrast. By taking these factors into account, a unit-less FOM was proposed to compare the overall sensing capability between different LSPR sensors, which is defined as the sensitivity S divided by linewidth FWHM.[16]

$$\mathrm{FOM} = \frac{S}{\mathrm{FWHM}}. \tag{9}$$

Given that the definition of the FOM also represents the variation of spectral intensity, LSPR sensing can also be reported by the scattering intensity variation $\mathrm{d}I/I$ of a single-color laser.[58] In this ratiometric scheme, the performance of the LSPR sensor can be defined as FOM*

$$\mathrm{FOM}^* = \frac{\mathrm{d}\lambda}{\mathrm{d}I} \cdot \frac{S}{I}, \tag{10}$$

where the narrower peak leads to a larger intensity change with equal amount of the peak shift. The FOM of the LSPR sensor is also proportional to its Q-factor, whose sensitivity is hampered by nonradiative Ohmic loss and radiative damping.

To date, the FOM of plasmonic structures serves as an important index for designing an LSPR sensor with higher sensitivity. The progress of FOM starts with ensemble nanoparticle synthesized by wet chemical approaches.[16,41–54] The LSPR peaks are non-homogeneously broad because of the non-uniformity of the sample, leading to a low FOM of 1–2. One way of addressing such a limit with regard to non-homogeneity is to synthesize a mono-dispersed sample. For example, Burgin *et al.* used uniform Au bipyramids and obtained an FOM of 4.5.[53] Another way to get rid of nonhomogeneity is to perform single particle experiments.[42,44,59] As shown in Fig. 1(a), McFarland *et al.* demonstrated that single silver nanoparticle with an FOM of 4.1 can be used to probe the molecules adsorbed onto the nanoparticle's surface, with a sensitivity reaching $\sim$ 100 zeptomoles.[42] The highest record of 5.4 was achieved with Au nanostar,[60] which was due to the sharp tip geometry that contains strongly confined local fields. FOMs are limited to less than $\sim$ 5 if strongly radiating plasmon modes are used.

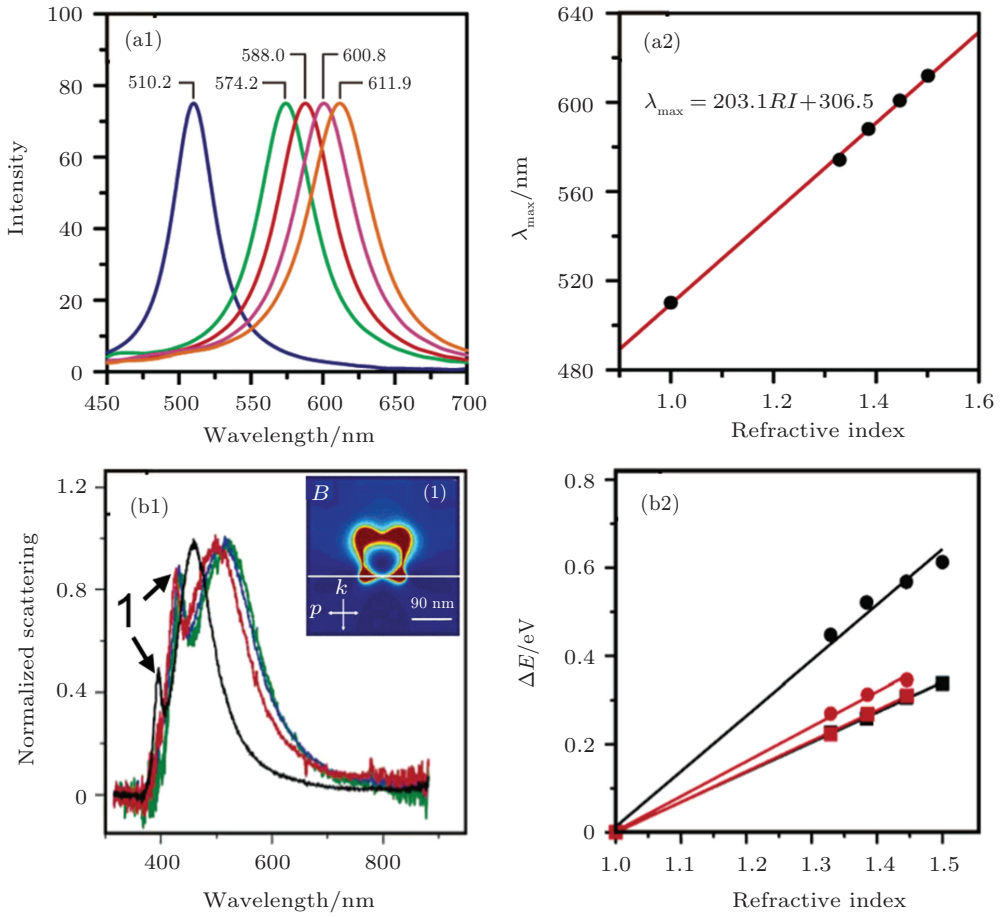


Fig. 1. (color online) FOM of individual nanospheres and nanocubes on a substrate. (a1) and (a2) LSPR peaks of a single Ag nanoparticle in different solvent environments, showing the linear relationship between the solvent RI and the LSPR wavelength, for which the FOM is 4.1.[42] (b1) and (b2) Scattering spectra of a Ag nanocube-on-glass in different dielectric environments. The narrower peak 1, quadrupole mode, sustains a sensing FOM of 5.4.[16] Reprinted with permission from Copyright 2003, 2005 American Chemical Society.

Further improvement of the FOM was realized by developing the nanostructure supporting dark plasmons. Dark plasmons cannot be directly excited by plane waves and so they are free from radiative damping. Therefore, dark plasmons can facilitate a narrower peak with FWHM significantly smaller than that of the bright modes. An efficacious way to utilize dark plasmons is to create Fano resonances,[17–20,22–24,26] featured as a dip in the scattering spectrum originating from the interference between bright (superradiative) and dark (subradiative) plasmons. An early experimental demonstration by Sherry *et al.* in 2005, showed that a high FOM of up to 5.4 can be achieved using a single nanocube-on-glass system[16] (Fig. 1(b)). Later on in 2011, Zhang *et al.*[23] noted that the substrate induced Fano resonance between the primitive dipole (bright) and quadrupole (dark) modes in

the nanocube accounted for the high FOM. The effect of RI serves to alter the strength of the interaction between the two modes, in addition to the dielectric screening effect in conventional LSPR sensing. After optimizing the spectral overlap between the bright and dark modes, the FOM of the substrate-supported nanocube system can theoretically be optimized to 20. Pronounced Fano resonance has also been experimentally realized in a Au nanodisk heptamer structure[20] with an FOM of 5.4, which is sensitive to the cluster size, geometry and local dielectric environment (Fig. 2(a)). The simulated FOM of the similar plasmonic sphere cluster can achieve a value up to 11.[18] Benefiting from the larger change in spectral contrast, a larger Fano dip can facilitate a higher sensitivity in response to the dielectric environment. Thus, the improvement in sensitivity of the Fano-based refractometric sensor always requires a larger Fano dip to achieve a higher spectral contrast. However, this is also accompanied by the broadening of the linewidth which in turn limits the FOM.[61]

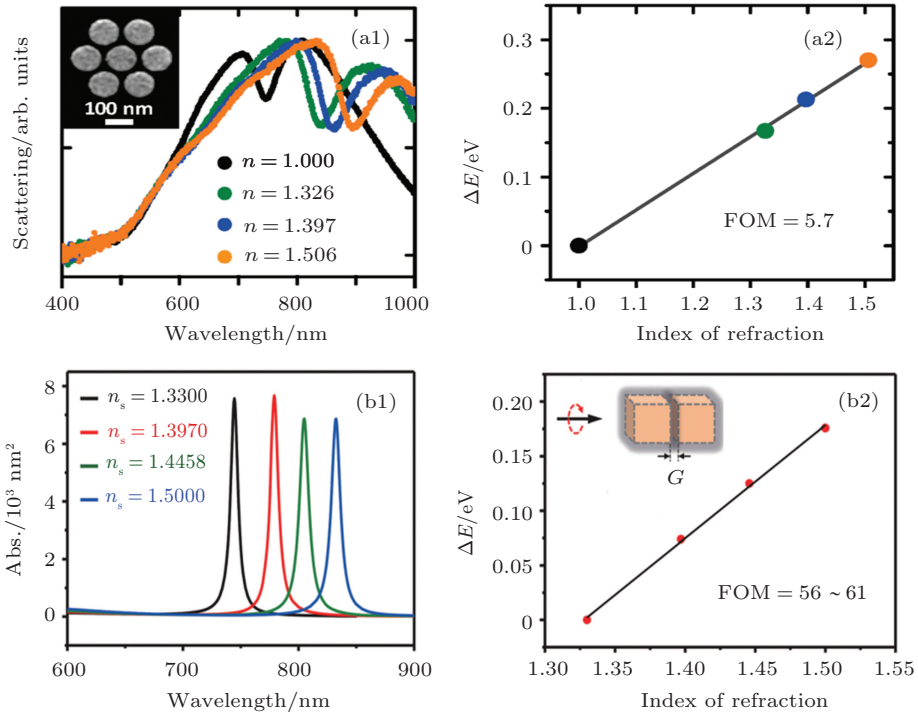


Fig. 2. (color online) Refractometric sensing using dark plasmons. (a1) and (a2) Experimental demonstration of Fano resonances in an Au nanodisk heptamer can sustain a sensing FOM of 5.7.[20] (b1) and (b2) Cavity plasmons in an Ag nanocube dimer exhibit an FOM of up to 61, approaching the ultimate limit of the sensitivity.[28] Reprinted with permission from Copyright 2010 American Chemical Society, Copyright 2016 Royal Society of Chemistry. The unit a.u. is short for arbitrary units.

A higher FOM can be obtained in a single nanorod geometry.[25,26] A high aspect ratio nanorod can be viewed as a Fabry–Pérot type cavity, where the SPP travels along the long axis and is reflected by two terminals. The resulting standing wave patterns on the nanorod defines the multipolar plasmon resonances based on the number of nodes. It was shown that higher order modes provide a higher FOM due to their narrower linewidth. Simulation predictions show that the FOM of the third order cavity mode is as high as 29. In 2016, Zhang *et al*. introduced a highly tunable dark plasmon for refractometric sensing with a sensitivity approaching the upper limit of any LSPR sensor.[28] (Fig. 2(b)). In their simulations, the dark mode was excited in a face-to-face nanocube dimer system, with an FWHM of only 17.6 meV, which is limited only by Drude damping. Similar to the nanorod cavity, the gap region of the nanocube dimer can also serve as a Fabry–Pérot-like cavity, where the SPP travel along the metal-insulator-metal (MIM) waveguide and are reflected at the nanocube edges.[27] Alternatively, from the plasmon hybridization point of view, this dark mode originates from the bonding coupling between the quadrupolar mode of one nanocube and the dipolar mode of the other. The FOM of this cavity mode can achieve an unprecedented high value of 61. The state of progress towards the improvement of the FOM of LSPR-based nanosensors is shown in Fig. 3(a). It can be approximately divided into four categories, i.e., assembled nanoparticles, individual nanoparticles, Fano resonances and dark (cavity) plasmons. In the quasi-static limit, the FOM of a pure LSPR for an individual nanostructure can be derived as:[14,62]

$$\mathrm{FOM} = \frac{|\varepsilon'_{\mathrm{m}}|}{n\varepsilon''_{\mathrm{m}}}, \tag{11}$$

where $\varepsilon'_{\mathrm{m}}$ and $\varepsilon''_{\mathrm{m}}$ are the real and imaginary parts of the metal-dielectric function. By interpolating the permittivity of Ag according to the J & C data, the energy-dependent ultimate FOM can be obtained as shown in Fig. 3(b). The FOMs of the cavity plasmons calculated from Fig. 2(b) are labeled as red spots in Fig. 3(b), indicating that its sensitivity almost approaches the theoretical limit. This suggests that the fabrica-

tion of improved nanostructures that support cavity plasmons is a promising direction of research for future ultrasensitive sensing applications.

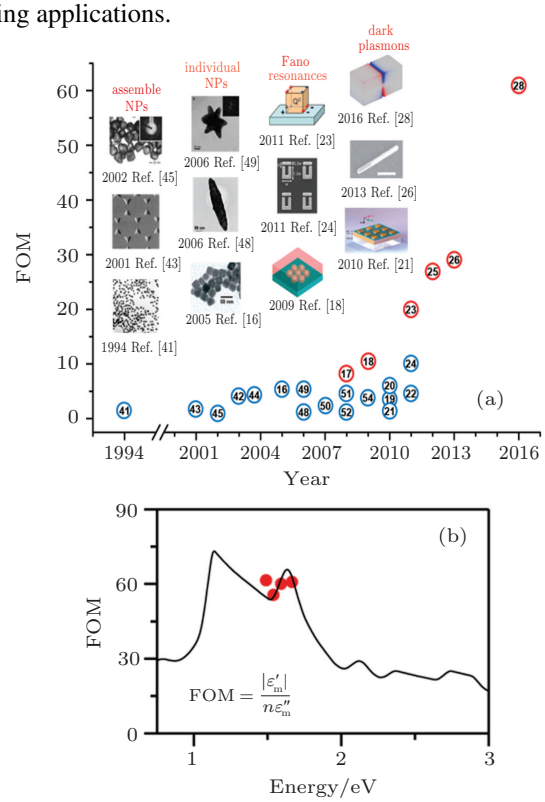


Fig. 3. (color online) Progress of FOM towards approaching the theoretical limit. (a) The FOM of LSPR-based sensors versus year, which is not a complete list but highlights the trend of FOM improvement. The blue (red) circles show the measured (calculated) results, where the numbers inside the circles represent the citation number of the appropriate references. (b) FOM of the cavity plasmons compared with the theoretically predicted FOM obtained by J & C permittivity,[28] which suggests that the cavity plasmons are approaching the ultimate sensitivity limit of the LSPR-based sensing. Reprinted with permission from Copyright 1994, 2001, 2002, 2005, 2006, 2009, 2010, 2011 American Chemical Society, Copyright 2016 Royal Society of Chemistry.

The aforementioned discussions mainly focused on the refractometric sensitivity contributed solely by the LSPRs. One of the most remarkable features of the LSPR sensor is that each individual plasmonic structure can work as an independent sensor. The lateral spatial resolution can be up to the single nanoparticle level, which inherently breaks the diffraction limit of light.[13] In fact, the FOM of plasmonic sensors can be substantially enhanced by at least one order of magnitude[63] by using lattice plasmons in periodically arranged plasmonic structures. Lattice plasmons originate from the diffractive coupling among the plasmonic elements. As a result, the FWHM of lattice plasmons is usually less than 10 nm, which significantly exceeds the theoretical limit of the pure LSPR peak.[64–66] As shown in Fig. 4(a), Yanik *et al.* obtained an extremely high FOM of 162 using subradiative collective modes with FWHM values smaller than 4.3 nm in a suspended nanohole array.[55] They also demonstrated how this ultrasensitive sensor can enable label-free sensing of monolayer proteins with the unaided eyes. Based on a similar principle, Shen *et al.* designed gold mushroom array plasmonic sensor with FOM up to $\sim$ 108, as shown in Fig. 4(b).[56] This array has also been used to detect cytochrome-c and alpha-fetoprotein with LOD as low as 200 pM and 15 ng $\cdot$ ml^{-1}, respectively. In addition to plane-wave excitation, the coupled nanostructures supporting Fano resonances can also be activated by SPP directed using a MIM waveguide near the nanostructures.[67] In these designs, the MIM waveguide is side-coupled with a pair of rectangular cavities, thereby forming a Fano dip with a resonance wavelength which depends on the cavity–cavity phase. A FOM of 56 was achieved in this case. Subsequently, the MIM waveguide has also been designed to be coupled with cavity resonators of various geometries,[68–70] such as double-stubs,[68] double-circulars,[68] and rectangular[69] cavities. In these simulation works, the FWHM of the Fano dips are $\sim$ 8 nm–20 nm with an FOM in the range of 55–77.

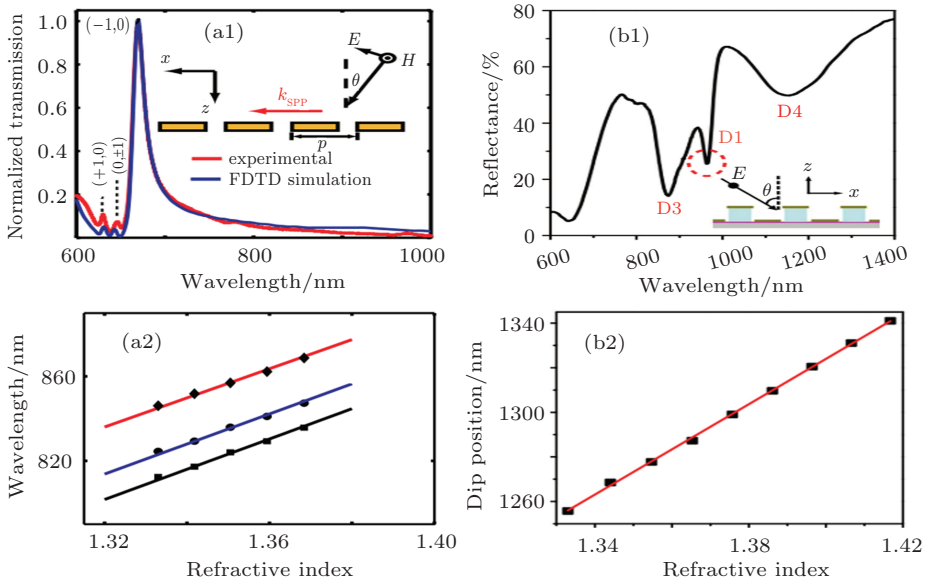


Fig. 4. (color online) Refractometric sensors using lattice plasmons. (a1) and (a2) Subradiative collective modes excited in a suspended nanohole array show extremely narrow peak with FOM reaching 164.[55] (b1) and (b2) Lattice plasmons obtained in gold mushroom arrays, with FOM of $\sim$108.[56] Reprinted with permission from Copyright 2011 National Academy of Science, Copyright 2013 Nature Publishing Group.

It should be noted that the significant improvement of the FOM of the lattice plasmons is at the cost of losing the nanoscale lateral spatial resolution when compared to individual LSPR-based sensors. This is because the lattice plasmons are delocalized collective modes associated with multiparticle long-range coupling or grating effects, excited by periodic plasmonic structures with large areas. On the other hand, the sensitivity to bulk RI changes of an SPR sensor is generally an order of magnitude higher than that of a lattice plasmon-based sensor.[13] However, by comparing the vertical field decay length between lattice plasmons and SPP, it can be determined that the higher FOM of propagating plasmons is at the expense of a lower vertical spatial resolution by approximately one order of magnitude.[71] A comparison of the LSPR mode, lattice mode, and SPP mode is shown in Fig. 5. The figure suggests that the choice of the sensing scheme is based on a trade-off between the sensitivity and the spatial resolution, where the key issue is the degree of light confinement among the different types of plasmon modes.

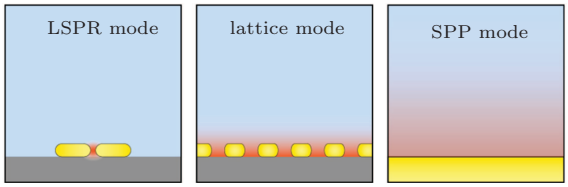


Fig. 5. (color online) Comparison of nanosensors based on LSPR, lattice plasmons and SPP. The higher the spatial resolution, the lower the FOM.

3.2. Spectral resolutions

In addition to FOM, spectral resolution is another key factor in determining the LOD in all of the spectrometric or ratiometric sensing schemes. In this case, the resolution is defined as three times the standard deviation of the noise that corresponds to a confidence level of about 90%.[72] Compared to the SPR sensor, the LSPR sensor benefits from a much smaller sensing volume and therefore suffers significantly less fluctuations due to the environment temperature or vibration.[71] Apart from these factors, the output noise that limits signal identification is mainly attributed to three types of noise sources:[73] (i) the intensity fluctuation of the light source, (ii) the shot noise that originates from the Poisson statistical photon flux, which can be effectively reduced by collecting more light under the saturation levels, and (iii) the inherent noise of the photodetector. In the case of spectroscopic sensing, all three noise sources can be effectively reduced by averaging time-series signals collected from the same detector (called time averaging). In this situation, the spectral resolution is proportional to the factor $\sqrt{M}$, where M is the number of the spectra to be averaged. Although simultaneously averaging the signals recorded from multiple detectors called spatial averaging, can improve the signal-to-noise ratio, it cannot suppress the light source noise. This is because the light intensity deviation affects all of the signal translation processes in the same way and needs to be suppressed by other methods. This drawback of spatial averaging is also reflected in the intensity-modulated ratiometric sensing scheme. This explains why the resolution of spectroscopic sensors is always higher than that of the ratiometric sensors.[15] A scheme based on the relative phase has also been used to improve spectral resolution, resulting in a higher FOM.[74]

To process the output signal, numerous algorithms have been developed.[75] Although most of them are created to readout the signal from a SPR sensor, they can also be straightforwardly applied to determine the spectral shift of the LSPR peaks in a similar manner. Beyond the simplest recognition method that directly reads the strongest point of a peak fitted by a Lorentz or Gaussian function, the most commonly used algorithms include the centroid method,[71,76–79] polynomial fitting,[71,76,80,81] optimal linear data analysis,[82] projection method,[83] integrated response technique,[84] *etc*. In the centroid method, the determination of the LSPR peak position is based on the calculation of the center-of-mass from the part of the peak above a certain baseline. The center-of-mass will be obviously affected by the noise of light intensity if a fixed threshold is set to an asymmetry peak. Thus modified strategies, such as dynamic,[77,78] weighted,[76] and fast[79] centroid methods have been developed to reduce the influence of light intensity fluctuations. Another well-known approach with a resolution comparable to the centroid algorithms is to fit the LSPR peak (above a certain threshold) using polynomial functions, where the peak position is determined by the extremum of the polynomial functions. Apart from calculating the shift of the peak maximum, some new strategies that utilize the asymmetrical shape changes of the LSPR far-field spectrum have been introduced to improve the spectral resolution based on the second order derivative spectrum, *e.g.*, monitoring the variation of the curvature[85] and inflection points.[86]

By applying the centroid and polynomial fitting algorithms using a fast 2 s integration time, Dahlin *et al*. demonstrated how to obtain a peak position with a precision higher than 5×10^{-4} nm and an extinction noise level lower than 5×10^{-6} absorbance units, respectively.[71] In their sensing scheme, the output noise was reduced based on a time averaging method using the highest light intensity before saturating the detector using the shortest integration time. The spectral resolution has been further improved towards $\sim 1 \times 10^{-4}$ nm with a longer integration time by Chen *et al*.,[87] where the signal was collected from a ~ 0.13 cm^2 area. However, the extremely high signal to noise ratio which resulted from these works relies on the spatially-averaged signal from large analyte areas, which is difficult to achieve in the case of individual plasmonic nanostructures.[58] In fact, the realization of single macromolecule detection with individual

plasmonic nanoparticles only requires subnanometer spectral resolution.[7–9] Further improvements for detecting smaller single-molecules are mainly hampered by the fluctuations attributed to Brownian movement in liquid environments during the protein-surfactant mixture process.[8]

3.3. Applications: strategies for improving the sensitivity

LSPR-based sensors mainly benefit from their nanoscale sensing volume due to the near-exponential decay property of the local field away from the structure surface. In terms of this feature, the LSPR-active nanostructures serve as a natural label-free molecular sensor for real-time detection of biomolecules and related kinetics processes without perturbing the analyte.[58,88] For molecular sensing, analyte binding events only result in local RI changes near the plasmonic surface. Therefore, compared with the FOM that represents the RI change of the total environment, a more comprehensive index called the $\mathrm{FOM_m}$ has been considered in the form of:[89]

$$\mathrm{FOM_m} \approx \mathrm{FOM} \cdot \exp(-2h_0/l_\mathrm{d})[1-\exp(-2h/l_\mathrm{d})], \quad (12)$$

where h is the size (thickness) of the molecule (molecule layer) covered on the plasmonic surface, h_0 is the distance of the analyte layer from the metal surface, which are both the dominant factors for the spectral change of the sensor; and l_d is the decay length of the plasmonic field that determines the sensing volume. The sensing volume can be measured by observing the spectral shift after depositing of dielectric layers of increasing thickness.[90] Generally, the spectral shift slows down when the surface coating exceeds ~ 20 nm,[91] an effective analyte height which is sufficient to probe macromolecules such as proteins. In case of probing of the trace molecules that cover the metal surface, the SPR and LSPR sensors show a similar sensitivity.[14]

As shown in Eq. (12), the FOM* associated with molecular sensing mainly relies on the coverage and thickness of the analyte over the surface of the nanostructures. This means that a large molecule, such as an antigen, antibody or enzyme, can produce larger spectral changes than a small molecule, resulting in a lower LOD.[92] Therefore, an effective strategy for improving the sensitivity is to increase the mass and size of the target analyte by binding extra macromolecules. On the other hand, the near-exponential decay performance of the local field suggests that the closer the analyte is to the plasmonic surface, the higher the sensitivity. Thus, the thickness of the bottom molecule layer used to selectively trap the analyte should be as short as possible. Haes *et al*. developed a biomarker detection scheme by capturing target molecules using a primary antibody on the surface of a LSPR sensor.[93] This resulted in a significantly improved sensitivity by the addition of a secondary antibody on top of the analyte, that caused the extra RI change (Fig. 6(a)). A similar strategy was implemented by Guo *et al*. with the design of an aptamer–antigen-antibody sandwich complex to probe the middle layer thrombin molecule.[94] The sensitivity has been further improved from 1.6 pM to 18.3 pM by using smaller DNA strands as the bottom capture layer to replace the traditional antibody, which allows the analyte to operate in a more sensitive regime (stronger local field). Given that the spectral shift is approximately proportional to the mass of the analyte, a straightforward approach for detecting small molecules depends on the realization of a high spectral resolution. Bingham *et al*. demonstrated a submonolayer detection of adsorbed water on the surface of ensemble Ag nanotriangles by applying high-resolution LSPR spectroscopy,[95] where the distinguishable LSPR peak shift was on the order of 10^{-3} nm. At this resolution level, the switching between different inert gases near the sensor's surface is also detectable (Fig. 6(b)).

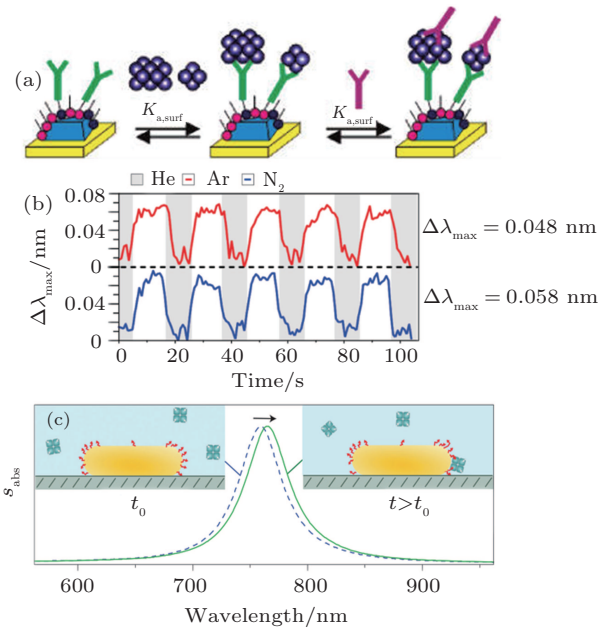


Fig. 6. (color online) Strategies for improving the molecular sensitivity (a) Increasing the analyte size by binding extra molecules.[93] (b) Small gas molecules detected using high-resolution spectroscopy.[95] (c) Single-molecule detection by photothermal microscopy.[9] Reprinted with permission from Copyright 2005, 2010 American Chemical Society, Copyright 2012 Nature Publishing Group.

Another effective sensing scheme for detecting small dye molecules is based on the coupling between plasmons and molecular resonances.[96–98] The spectral shift caused by the dye molecule binding event is significantly amplified when the molecular absorbance overlaps with the LSPR of the nanostructures to some degree. Zhao *et al*. exploited the fact that small camphor molecules can generate amplified LSPR shifts by tuning the LSPR near the resonance of a CYP101 protein,[97] in which case the average shift per camphor molecule was ~ 0.07 nm. Apart from camphor molecules, Rhodamine 6G[98] and MgPz[96] molecules also exhibit similar effects that cause a pronounced spectral shift, demonstrating the possibilities for sensitive detection of a wide range of small dye molecules.

Improving molecular sensitivity is one of the major efforts in the application of LSPR sensors. This requires a discernible spectral response to facilitate reporting on analytes with a smaller size (thickness), lower weight or lower molecule number. In recent years, the LOD of individual LSPR sensors have improved from, *e.g.*, $\sim 6 \times 10^4$ hexadecanethiol,[42] ~ 700 streptavidin molecules,[99] to $\sim$ 360 neutravidin,[100] ~ 18 streptavidin molecules,[101] and has finally now toward the single-molecule level[7–9] — the ultimate limit in analytic chemistry and biology. Mayer *et al*. were the first to achieve label-free single-molecule detection based solely on the observed LSPR peak shift using a statistical approach. They found that a single protein was distinguished by a 0.34-nm spectral blueshift, which was analyzed upon antibody-antigen binding events that occurred near the tip area of an individual gold bipyramid.[7] The corresponding simulations that treat proteins as small dielectric spheres also show a similar blueshift (< 0.5 nm). Ament *et al*. developed a continuous single-molecule LSPR sensing scheme by using an intense white light laser source and a stable optical setup with individual Au nanorods.[8] In terms of a wavelength histogram analysis, the single unlabeled protein binding event that causes ~ 0.3-nm spectral shift can be characterized in real-time. In their experiments, the time resolution approached the millisecond scale, which is several orders of magnitude better than previous works. By choosing individual small nanorods (37 nm $\times$ 9 nm) that allowed the volume of the plasmonic mode to be comparable to that of the analyte protein, Zijlstra *et al*. demonstrated a single-molecule detection with the molecular weight as low as to 53 kDa[9] (1 Da $= 1.66054 \times 10^{27}$ kg) (see Fig. 6(c)). To overcome the poor scattering efficiency of the small nanorods, they applied a sensitive photothermal microscopy approach to detect the weak spectral response of the single-molecule binding events. In the photothermal assay, an absorbance dependent thermal lens was created by pump laser heating. The binding events change the absorbance of the nanorod which results in a variation of the thermal lens, and this leads to an intensity change of the probe beam. They demonstrated that the sensitivity of the photothermal assay was two orders of magnitude higher than that of conventional scattering methods.

4. Displacement sensing — plasmon rulers

4.1. Universal scaling based on plasmon hybridization

The aggregation of nanoparticles in noble metal colloids leads to color changes of the solution, resulting from the appearance of dramatic red-shifted broad peaks that dominate the far-field spectrum.[102] Early in 1997, this plasmonic coupling-based feature had been utilized to selectively probe oligonucleotides with the LOD down to 10 fM.[103] The further progress of chemical and biological applications involving the self-assembly and aggregation of nanoparticles has been comprehensively discussed in the review article of Saha *et al*.[104]

The plasmonic response of the coupled nanostructures can also be quantitatively modified by tuning the gap distance between the structures. This gap-distance dependent plasmonic response can be developed as 'plasmon rulers' to monitor nanoscale interparticle distances or distance changes, by observing the optical spectrum of the coupled nanoparticles.[105] In order to apply the plasmon ruler for displacement sensing applications, it is necessary to calibrate the LSPR peak position as a function of the interparticle separation. Su *et al*. reported a phenomenological law related to this gap-distance dependent interparticle coupling effects.[57] They measured the scattering spectra of lithographically fabricated elliptical disk pairs with various sizes and gap distances and demonstrated that the LSPR peak shifts follow a near-exponential function in relation to the interparticle distance (Fig. 7(a)). After normalization of the gap distance (spectral shift) to the nanoparticle size (LSPR wavelength), they discovered that the nanoparticle pairs with different sizes follow the same exponential decay function. Similar approaches based on both wet chemical synthesis and lithography technology were performed by Gunnarsson *et al*.,[106] which also verified this near-exponential behavior in the nanoparticle pair systems. Furthermore, as shown in Fig. 7(b), Jain *et al*. demonstrated that this near-exponential decay trend is a universal scaling behavior of plasmon coupling. It can be applied to all nanoparticle pair systems with different nanoparticle sizes, shapes, metal types, and dielectric properties of the surrounding medium.[107] In addition to these definitive investigations, the plasmon ruler behavior has also been well examined for various nanostructure pair systems with different geometry, such as nanospheres,[108] nanorods,[109,110] nanocubes,[111] nanoshells,[112] *etc*., whose plasmon shifts were observed by extinction, scattering, absorption, or even EELS.[113] Generally, the properties of the plasmon ruler can be expressed as an empirical equation in the form of:

$$\frac{\Delta\lambda}{\lambda_0} \approx A \cdot \exp\left(-\frac{d/D}{\tau}\right), \tag{13}$$

where λ_0 is the LSPR wavelength of the isolated nanoparticle, $\Delta\lambda$ is the wavelength shift of the coupled plasmon mode relative to the λ_0, $\Delta\lambda/\lambda_0$ represents the fractional spectral shift, d is the surface-to-surface spacing between the nanoparticle pair, and D is the size of the nanoparticle. The near-field coupling effect of nanoparticle pairs starts to appear when $d/D < 2.5$–3. A is the amplitude of the shift at zero spacing, which depends on the size, shape, and dielectric constant of the metal and the surrounding environment. A higher A implies a larger spectral shift with equal distance change. τ is the exponential decay length, which represents the effective volume of the local field. In most spheroidal geometries, the decay length τ is approximately 0.2, which is independent of the size, medium, and metal type, but in other geometry cases, this tendency is not fully clarified.[114]

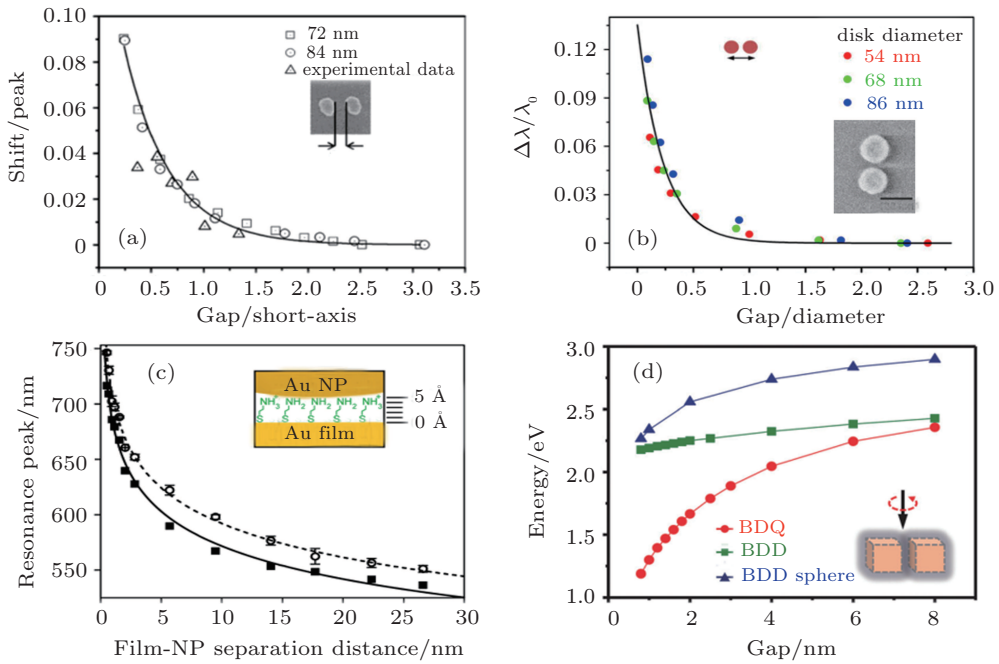


Fig. 7. (color online) Universal near-exponential decay behavior of different plasmon rulers. (a)–(c) Radiating antenna plasmons in elliptical nanodisk dimer[57] (a), nanodisk dimer[107] (b), and NPOM[115] (c). (d) Cavity plasmons in nanocube dimer system.[28] Reprinted with permission from Copyright 2003, 2007, 2012 American Chemical Society, Copyright 2016 Royal Society of Chemistry.

In essence, the near-exponential decay performance of the plasmon ruler can be well understood in a physically intuitive manner called the plasmon hybridization model.[116–118] This model is rigorously analogous to the molecular orbital theory: the molecular orbital results from the hybridization of individual atomic wave functions. In the simplest case of two adjacent nanoparticles[117] separated by a distance d larger than the diameter of the nanoparticles, the nanoparticle dimer can be approximated as bonded classical dipoles (with angular momentum $l = 1$) through Coulomb interaction. The hybridization of the dipoles results in red-shifted low-frequency bonding (blue-shifted high-frequency antibonding) dipole plasmon mode, such that the shifts are symmetric and follow a $\sim 1/d^3$ relationship. The bonding dipole mode originates from two individual dipoles moving in phase, leading to a large net dipole moment that can be effectively excited by light. This collective mode is therefore called the bright mode or radiating antenna mode, that always dominates the far-field spectrum. In contrast, the antibonding dipole mode which results from the interaction of two anti-aligned dipole moments, exhibit almost null net dipole moment and thereby cannot be directly excited by a plane wave. This mode is known as the dark mode, which is almost invisible in the scattering spectrum but sometimes can still be found in absorption cases. As d becomes smaller, the dipole plasmon of one nanoparticle starts to couple with the higher multipole plasmons ($l > 1$) of the other nanoparticle, which involves higher powers of $1/d$, *i.e.*, quadrupoles with $1/d^5$, octupoles with $1/d^7$, *etc*. By taking all these terms into account, the resulting plasmon shift will exhibit a near-exponential decay, which is much faster than that predicted by the dipole-dipole coupling, since d is significantly smaller than D. On the other hand, with a small d, the higher order bonding plasmon modes also start to carry the moment from the dipole plasmon due to the plasmon hybridization, and is therefore visible in far-field scattering spectrum. Note that all these features are based on the case that the polarization of light aligns with the dimer axis. For perpendicularly polarized excitation, the far-field spectrum exhibits a very weak blueshift of the collective plasmons because the effects of the plasmon hybridization are much smaller.[119]

4.2. Improvement of displacement sensitivity

According to the nonlinear trend of the plasmon ruler equation, the decrease of the gap distance results in an increasing redshift of the bonding plasmon mode. This implies that a higher displacement sensitivity can be obtained for a smaller gap distance. This sensitivity is dramatically improved when the plasmon ruler is applied to a gap distance smaller than 5 nm. However, the fabrication of such a narrow gap is a challenging task when considering current nanofabrication technologies with regard to spatial control of the interparticle separation, with sub-nanometer accuracy in three dimensions. Benefiting from the highly uniform size and shape in the fabrication of nanoparticle dimers with various geometry, the lithographic pattern method plays a primary role in systematically understanding and calibrating the performance

of plasmon rulers over a wide spacing range. However, this method suffers from serious limitations in regards to fabricating the gaps and their interval is significantly narrower than ~ 5 nm.[114] Moreover, these lithographic fabricated patterns are naturally fixed on the substrate, which hampers their use as displacement sensors. Colloidal synthesized nanoparticle dimers with narrow gaps linked by molecules can overcome the aforementioned limitations in principle. However, they are still limited because of the complexity of the analysis which must be performed, *i.e.*, optical identification of the individual dimers and their steric configuration from other multi-nanoparticle complexes based on light polarization studies and electron microscopy.

A simple approach to minimizing the preceding complex issues for the development of a well-controlled narrow gap is to place a nanoparticle in close proximity to a metal mirror, thereby forming a nanoparticle-over-mirror (NPOM) system. The NPOM system can be modeled as a plasmon hybridization between the nanoparticle and its electromagnetic image induced within the metal mirror,[118] whose optical behavior closely resembles the dimer system in some aspects. In the NPOM setup, the gap distance can simply be tuned down to an atomic length scale by functionalizing an organic/dielectric spacer layer on the metal mirror (or the surface of the nanoparticle) with varying thickness. Furthermore, every nanoparticle situated on top of this spacer layer is naturally created as a plasmon ruler with uniform particle-film separation and a spatial orientation, which can be easily extended to large area applications and significantly simplify the experimental characterizations. In comparison with the dimer system, the bonding plasmon mode in the NPOM shows a larger peak shift in response to equal changes of the gap distance. This is because the contributions from higher-order angular momentum states of the NPOM plasmon are stronger than that of the dimer case.[102] Hill *et al*. experimentally investigated the plasmon ruler properties of the NPOM system and its displacement sensitivity in a very narrow gap region.[115] The NPOM is spaced by an organic layer with a thickness ranging from 2 nm to 0.5 nm, where the smallest interval can down to that of a single C–C molecular bond (~ 0.18 nm). At the narrowest 0.5-nm separation, the displacement sensitivity can up to a 5 nm peak shift per Ångström thickness change (5 nm/Å, shown in Fig. 7(c)). They indicated that this level of sensitivity approaches the limit of the radiating antenna plasmons.

Recently, it has been theoretically predicted that for narrow gap distance, the cavity plasmons have the potential to be used in displacement sensing with a sensitivity significantly higher than that of the radiating antenna plasmons. As shown in Fig. 7(d), Zhang *et al*. calculated the plasmon ruler behavior of the cavity plasmons in an adjacent Ag nanocube pair.[28] They found that the peak shift of the cavity plasmon mode can achieve a theoretical value of 35 meV as the interparticle separation is varied from 1.6 nm to 1.5 nm, equivalent to 19 nm/Å. However, the cavity plasmon is a dark mode that is almost invisible in dark-field scattering spectroscopy, which is not as convenient as using the radiating antenna mode for a wide variety of applications. In analogy to the nanocube dimer system, the cavity plasmons can also be excited in other mirror-coupled nanostructure geometry with two adjacent parallel flat surfaces, such as the nanocube-on-mirror,[120] and nanowire-on-mirror (NWOM).[121] Because of their reduced symmetry, the cavity plasmons supported in their nanocavities are quasi-dark modes. They can be effectively excited by a plane wave, resulting in a strong peak appearing in the scattering spectrum, at the cost of slight broadening of its FWHM. This feature makes the mirror-coupled nanostructure geometry a promising system to conveniently utilize the cavity plasmon for realistic sensing applications. Recently, the outstanding displacement sensitivity of the cavity plasmon was experimentally demonstrated by Chen *et al*. in two metalic NWOM systems[121] (Fig. 8). They developed a gold NWOM system consisting of a 0.5-nm-thick ligand-covered AuNW situated on top of an Al_2O_3 thin layer coated on an ultra-smooth Au film. By observing the spectral shift when the thickness of the Al_2O_3 layer was varied from 5 nm to 0.5 nm, they found that the cavity plasmon also obeys the universal near-exponential decay behavior. The unprecedented displacement sensitivity of 14 nm/Å was obtained at the nanowire-film distance of ~ 1 nm (Fig. 8(a)), which is about three times higher than the best experimental result obtained using the radiating antenna mode (5 nm/Å). The higher sensitivity of the cavity plasmons results from the greater contributions from higher order modes. In another point of view, the cavity plasmons confine more light into the analyte film compared to the radiating antenna plasmons. Furthermore, they also developed a silver NWOM system by directly depositing a 2.3-nm-thick PVP covered AgNW on an Au mirror, while performing *in situ* probing of small thickness changes of the PVP layer induced by thermal expansion effect (Fig. 8(b)). By fully utilizing the spectral resolution (0.01 nm) of the spectrometer, they demonstrated that the vertical differential resolution of the cavity plasmon can be pushed toward 0.58 picometer, which corresponds to a 0.069 nm spectral shift. This sensitivity significantly exceeds the existing Ångström-scale differential resolution, which may facilitate new possibilities in the development of ultrasensitive sensors to monitor very weak physical or chemical processes in atomic thickness materials.

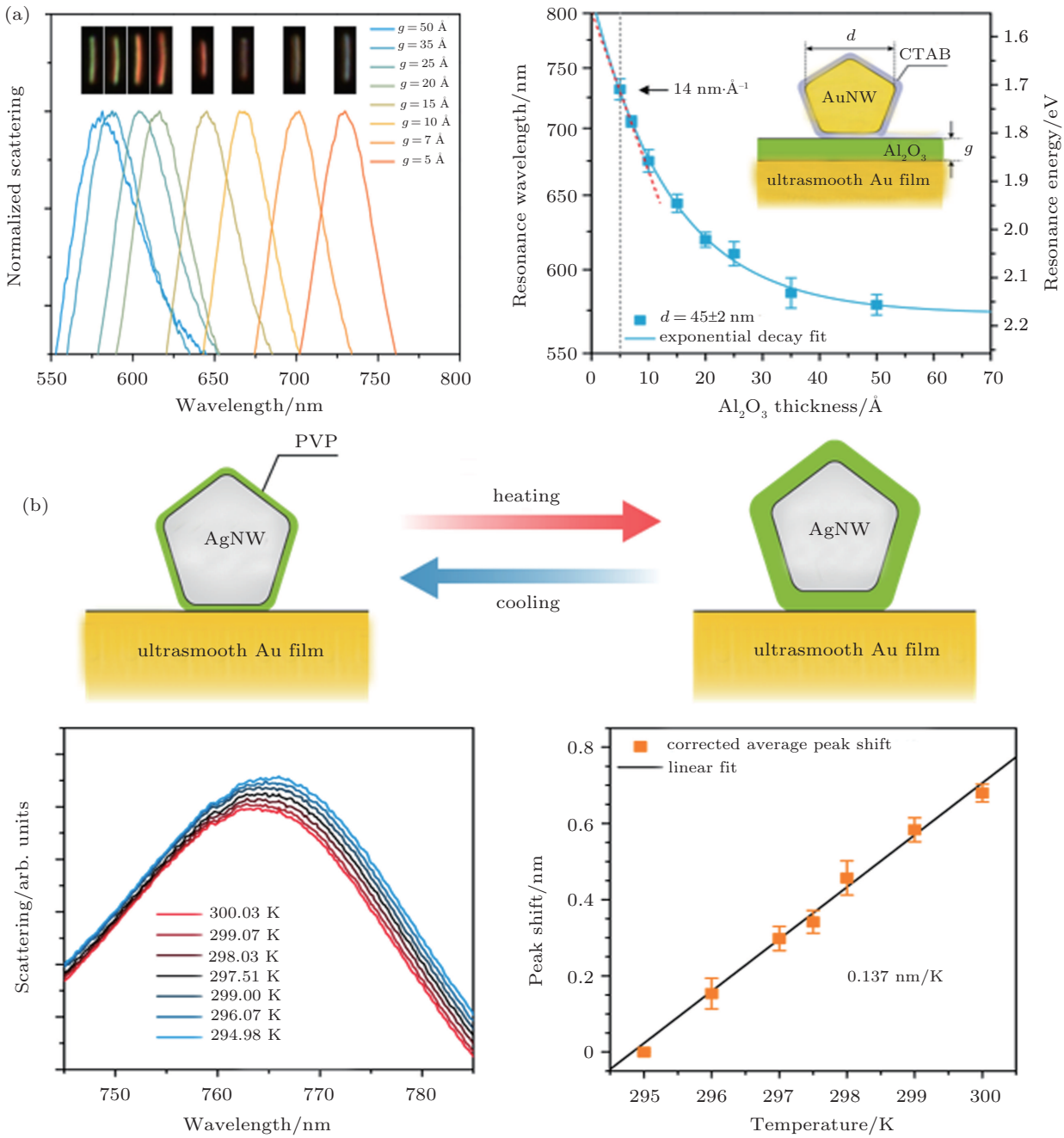


Fig. 8. (color online) NWOM plasmon rulers using cavity plasmons.[121] (a) Near-exponential decay performance of the cavity plasmons with sensitivity reaching 14 nm·Å^{-1}. (b) Cavity plasmons applied in thermal expansion experiment for *in situ* probing of thickness changes with a resolution up to 0.58 picometer. Reprinted with permission from Copyright 2018 Nature Publishing Group.

According to the classical Maxwell descriptions, both the plasmon hybridization model and the universal scaling performance of the plasmon ruler suggest that the displacement sensitivity increases monotonically as the gap distance decreases, thus encouraging the development of plasmon rulers with ever narrower gaps. However, recent progress both in theoretical[122] and experimental[123,124] studies suggest that the classical electromagnetic model fails to predict the plasmonic behavior over very narrow gap distances (especially at the sub-nanometer scale) due to the emergence of quantum mechanical effects, such as nonlocal screening and electron tunneling. In the quantum regime, the bonding plasmon modes show slower wavelength redshifts and finally vanish, along with the appearance of a charge transfer plasmon before the gap distance is reduced to zero.[125] This means that the quantum effects set the ultimate limits on the displacement sensitivity, where the maximum sensitivity is obtained at the narrowest gap before the electron tunneling becomes dominant. According to the quantum corrected model,[122] the electron tunneling probability not only depends on the width of the gap junction but also on the conductivity in the gap junction. Vacuum or air junctions have the lowest elec-

trical conductivity, and the tunneling effect usually occurs below a 0.5 nm gap distance.[124] For the cube dimer structure using 1,4-benzenedithiolates (BDT) as a spacer layer with a larger conductivity,[126] the charge transfer plasmons appear at $\sim$ 1.3-nm gap distance. Lerch *et al*. studied the plasmon ruler behaviors of a DNA linked Au nanoparticle dimer system by varying the DNA length.[127] They found that the plasmon ruler followed the universal exponential decay function when the gap distance was larger than 2.8 nm. For a shorter gap width, the emergence of quantum mechanical effects strongly modifies the response of the bonding plasmon mode, whose shifted resonance wavelength depends on the gap morphology. This transformation gap distance reaches $\sim$ 2.8 nm due to the higher conductivity of the DNA spacer layer. Therefore, in order to obtain a higher displacement sensitivity, the conductivity of the gap region in the plasmon ruler should be as low as possible, so that the plasmon ruler can operate in a narrower gap distance before the emergence of quantum mechanical effects.

4.3. Complex structural and spectral changes

The aforementioned plasmon ruler systems mainly focus on the LSPR peak shift caused by the change in the gap distance in dimer-like systems. In this section, we will introduce more complicated systems, where the relative displacement or deformation of the plasmonic elements cannot solely be described by one-dimensional gap distance variations. In this case, the plasmon modes used to represent structural deformation mainly utilizes Fano resonances. The spectral properties of the Fano resonance for plasmon ruler systems can be approximately divided into three types: (i) a fixed Fano dip wavelength with varied linewidth, which can be viewed as the opposite shifts of two adjacent peaks, or radiance sensing monitoring of the depth of the dip, (ii) a fixed Fano dip with a varied broad superradiant peak, and (iii) the wavelength, width and depth of the Fano dip are all changed. The most complicated case includes both the peak shift and the radiance change. Hentschel *et al*. designed a plasmonic nanodisk heptamer, and showed that the Fano resonance originated from the coupling between the center nanodisk and the other surrounding elements.[128] By decreasing the relative separation among all of the nanodisk elements, they found that a continue redshifted Fano dip with an increase in depth starts to appear due to the strong inter-disk coupling. This coupled structure could be viewed as a plasmon ruler for sensing the in-plane stretching or breathing mode of the substrate beneath. Shao *et al*. developed an individual Au nanorod–nanosphere core-satellite system,[129] where the presence of small Au nanoparticles results in the symmetry breaking of the nanorod's electromagnetic environment, thereby significantly modifying the spectral shape. The plasmonic responses associated with the Fano resonance are sensitive to the position and gap distance of the Au nanoparticle with respect to the nanorod, which can serve as a two-dimensional polar-coordinate-based plasmon ruler. Gallinet *et al*. reported on a dolmens-like nanostructure consisting of an individual cuboid suspended on top of a side-by-side separated nanorod dimer,[61] where the cuboid (nanorod dimer) supports the strong radiative dipolar (non-radiative quadrupolar) mode. In-plane movement of the top cuboid with respect to the center of the nanorod dimer leads to the appearance of an LSPR dip with varied FWHM and intensity, which originated from the plasmonic dipole-quadrupole coupling effect (Fig. 9(a)).

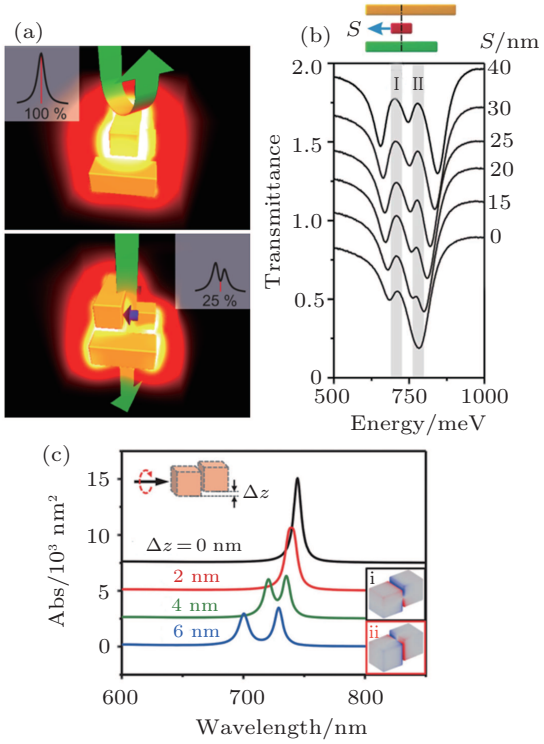


Fig. 9. (color online) Plasmon rulers associated with symmetry breaking. (a) Displacement sensors based on a radiative sensing scheme.[61] (b) Three-dimensional displacement sensing based on Fano resonance.[130] (c) Displacement sensing in vertical and horizontal directions measured via the spectral shift and splitting of the cavity plasmons.[28] Reprinted with permission from Copyright 2013 American Chemical Society, Copyright 2011 American Association for the Advancement of Science, Copyright 2016 Royal Society of Chemistry.

By observing the radiance change at the dip wavelength instead of relying on the wavelength shift, they demonstrated that this coupling feature can be used for structural sensing with Ångström scale displacement sensitivity. As shown in Fig. 9(b), upon further addition of a side-by-side separated cuboid dimer on top of the aforementioned dolmens-like nanostructure, Liu *et al*. achieved a three-dimensional displacement sensing scheme by plasmonic quadrupole–dipole–quadrupole coupling.[130] In-plane displacement sensing is achieved by *y*-axis detuning of the middle rod, which gives rise to the appearance and shift of the 1–3 LSPR dips. The detection of out-of-plane movement relies on the vertical shift of

the middle rod with respect to the middle position of the two rod pairs, which can be monitored by the spectral change of two LSPR peaks with the performance different relative to the in-plane case. Recently, Zhang *et al*. designed an Ag nanocube dimer system based on plasmonic bonding quadrupole–dipole coupling, forming the lowest order cavity plasmon.[28] They found that the parallel offset between the nanocubes along the plane perpendicular to the dimer-axis cause the splitting of the cavity plasmons into two blue-shifted modes with different shift speeds (Fig. 9(c)). Therefore, this cavity-plasmon-based system can also be viewed as a three-dimensional plasmon ruler with a much simpler geometry and higher sensitivity. The displacement parallel to the dimer-axis can be probed by the wavelength shift of the plasmon mode (as introduced in Subsection 4.2), and the relative translation normal to the dimer-axis can be detected by observing the spectral shifts of the two split peaks.

4.4. Applications

In 2005, Sönnichsen *et al*. first applied the concept of the plasmon ruler to chemical and biological sensing.[105] They developed single pairs of metal nanoparticles linked by flexible DNA tethers. Changes of the interparticle distance were triggered by the events of DNA hybridization, which were reported in real-time by measurement of the spectral shift of the LSPR peak (Fig. 10(a)). They demonstrated that the effective sensing distance range can reach 70 nm with a continuous monitor time in excess of 3000 s. Since then, plasmon rulers have served as a bleaching-free and nonblinking tool for probing dynamic interparticle displacement induced by various physical, chemical and biological processes.[131] One of the most widely used plasmon ruler systems is based on a DNA bridged metal nanoparticle dimer structure, involving biophysical conformation, dynamic biological processes based on enzyme reactions, *etc*. For instance, Morimura *et al*. developed a double-stranded DC5 DNA linked nanoparticle dimer as a plasmon ruler[132] to observe DNA conformational changes at the nanoscale due to transcription factor binding processes. In addition to the bending, the cleavage of the DNA in the presence of the restriction enzyme EcoRV can also be observed using DNA linked plasmon rulers with a temporal resolution up to 240 Hz.[133] Based on a similar system, the stiffness of DNA inside the interparticle gap region has been investigated.[134] The thermal displacement between the nanoparticles can be analyzed by continuously monitoring their spectral fluctuations. This DNA linked nanoparticle dimer geometry has also been used for *in-situ* monitoring of the extension process of DNA after the introduction of telomerase,[135] where the activities of this enzyme in HeLa cells could be examined at the single-molecule level. Similar DNA or RNA extension/striction processes associated with ribonuclease,[136] bovine serum albumin,[137] DNA binding protein,[138] and salt solution[139] have also been reported. These processes can in turn be utilized to detect the target molecules that cause the regulation of DNA, *e.g.*, as demonstrated by Guo *et al*., the LOD of target molecules in PBS and human serum reach 10^{-13} M and 10^{-11} M, respectively.[140]

Due to the pronounced bright color spot that can be detected using a microscope with excellent photophysical stability even in a complex environment, plasmon rulers also serve as a powerful platform for elucidating the complex transient interactions and dynamic biological processes that occur in living cells. The intra-/extra-cellular position and interparticle distance of plasmon rulers can be determined by simple light-scattering microscopy. Lee *et al*. demonstrated the specific and reversible detection of single matrix metalloproteinase molecules secreted from mammary epithelial live-cells by DNA-linked nanoparticle pairs.[141] In their experiments, the binding of target molecules onto DNA aptamers resulted in changes of the interparticle distance (Fig. 10(b)). Rong *et al*. reported on a plasmon-ruler-based approach for real-time characterization of the dynamic profiles of the membrane of living HeLa cells.[142] The nanoparticles were used to label the cell's surface using fibronectin–integrin complexes. Thus, relative induced displacement of the nanoparticles due to the fluctuations of the membrane can be monitored in real-time by changes in the resultant spectral intensity. They further improved this technique to realize a more comprehensive characterization of the detailed structural heterogeneity of individual cell membranes.[143] The involvement of the protease enzyme caspase in apoptotic signaling in live cells has also been widely researched using plasmon rulers. Jun *et al*. reported on the characterization of early-stage caspase-3 activation by inserting DEVD-sequence-bridged nanoparticle clusters into live cells,[144] where the caspase-3 can cut the DEVD sequences resulting in a spectral change due to the cleavage of the clusters. Further studies on the role of caspase in live cells have been performed by Tajon *et al*.[145] They designed a peptide sequence linked plasmonic core-shell nanoparticle dimer to detect caspase-3 activity and trajectories with a single-molecule resolution and a wide dynamic range, for 10 ng of total protein in drug-treated K562 cell lysates (Fig. 10(c)).

In addition to biological assays, the concept of plasmon rulers has also been widely utilized for various physical and chemical applications including color switching,[146] gas sensing,[121,147] as strain force transducers,[148,149] pH sensing,[149] *etc*. For example, Powell *et al*. developed a thin fluoropolymer spaced nanocube-on-mirror system as a plasmonic humidity sensor.[147] An increase in humidity leads to the swelling of the fluoropolymer via strong water adsorption from its surroundings, which is reflected in a spectral redshift of the cavity plasmons. The authors demonstrated that this

plasmon ruler system was capable of a maximum sensitivity of 0.57-nm peak shift per relative humidity change. However, this sensitivity was achieved by varying the polymer thickness from 11 nm to 24 nm, a gap distance range which had not previously exhibited the advantages of the cavity plasmon harbored in narrow gaps. To achieve a higher sensitivity of the cavity plasmon, Chen *et al*. designed a NWOM system for sensing water molecules, where the spacer analyte film used to adsorb these molecules was only 2-nm thickness.[121] They determined that the sensitivity could be increased up to 1.28-nm peak shift per relative humidity change (Fig. 10(d)). The thinner analyte film benefits from the higher sensitivity of the plasmon ruler, but suffers from a lower capacity of the adsorbed molecule. Therefore, cavity plasmon-based sensors seem to be more suitable for trace molecule detections.

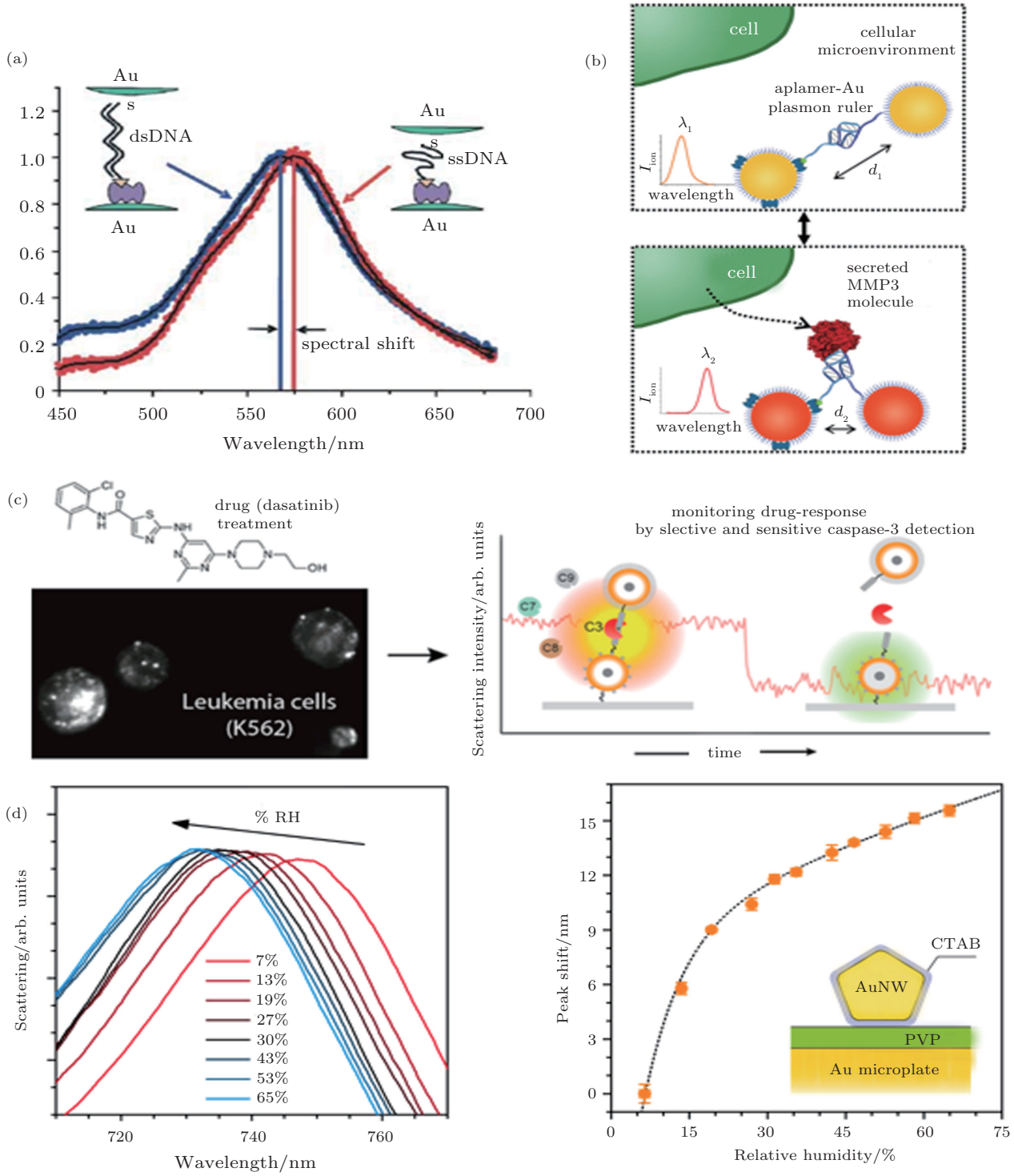


Fig. 10. (color online) Some typical applications using plasmon rulers. (a) Monitoring of DNA hybridization events using nanoparticle dimer.[105] (b) Detecting MMP3 proteins secreted from live cells.[141] (c) Probing of drug response by selective detection of caspase-3 in live cells.[145] (d) Cavity plasmon-based humidity sensing resulting from the thickness change of a PVP layer filled inside the NWOM cavity.[121] Reprinted with permission from Copyright 2005 Nature Publishing Group, Copyright 2015 American Chemical Society, Copyright 2018 Nature Publishing Group.

5. Other LSPR-based sensing

5.1. Chiral sensors

The chirality of an object can be interpreted as a mirror image which does not coincide with the original object. A chiral material shows different complex dielectric functions under right- or left-handed illumination. On one hand, the difference of the imaginary part leads to the different absorptance of the right or left circularly polarized light, which is known as the circular dichroism (CD). On the other hand, the difference associated with the real part causes the phase change of these two circularly polarized components to be different. As a result, linearly polarized light will be rotated after passing through a chiral medium, where the linearly polarized light serves as the superposition of right- and left-handed light. This phenomenon is known as optical rotatory dispersion (ORD). Many biological molecules exhibit chirality, such as amino acids, carbohydrates, nucleic acids and proteins, and many of them only express one handedness. Therefore, the CD and ORD spectra are powerful methods for revealing the secondary structure of macromolecules as well as their deformation and dynamics.[150] However, the measurement of the CD and ORD of the high chirality biological molecules and materials require a high concentration or a large volume of analyte due to their very weak optical chiral response. Probing trace amounts of chiral molecules requires signal amplification, which can be effectively realized using LSPR,[151–153] *e.g.*, by combining chiral plasmonic structures with chiral molecules. In such hybrid chiral systems, the CD response of the chiral molecules was modified, or the CD response occurred in the ultraviolet wavelength (the chiral molecules' region) to the visible wavelength (the LSPR's region). Maoz *et al*. demonstrated a CD response for two-layer chiral molecules covering the surface of a plasmonic structure,[154] whereas the natural chiral optical response of the molecules themselves was unmeasurable. As shown in Fig. 11(a), Lu *et al*. discovered that the CD response of DNA molecules can be two orders of magnitude larger after they are combined with individual Ag nanocubes.[155] Zhang *et al*. simulated the CD response of a chiral molecule inside the gap region of a dimer pair, and discovered that a significantly amplified molecular CD originated from the strong Coulomb interaction.[29] They also indicated that the giant CD was caused by the field enhancement of the LSPR when the molecular dipoles are parallel to the dimer axis. Wang *et al*. also demonstrated that the CD can be modified by tuning the symmetry of the system, the interparticle distance, and the dielectric environment.[156] In addition to the field enhancement, the design of a plasmonic structure to support intense near-field chirality can also enlarge the molecular CD.[157,158] This is because the interaction efficiency between the circularly polarized light and the chiral molecule is enhanced by orders of magnitude.

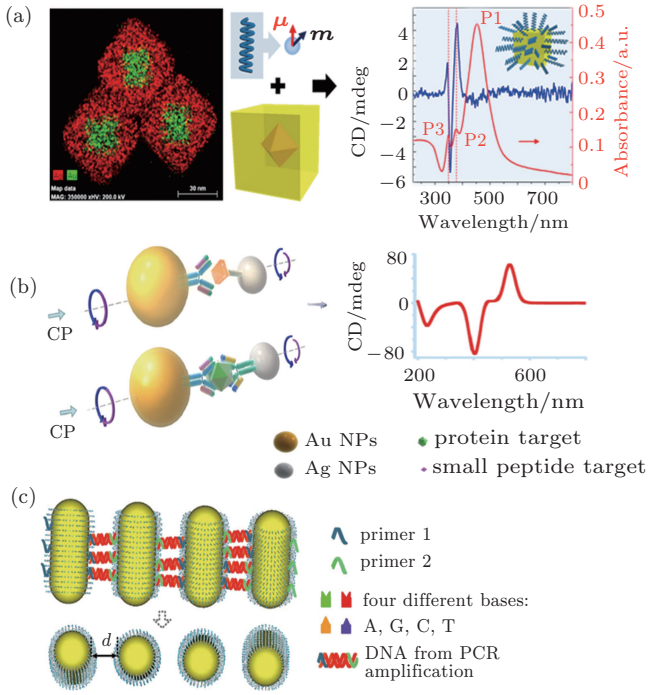


Fig. 11. (color online) LSPR-based chiral sensing. (a) Improvement of the CD response of the chiral molecule by plasmonic field enhancement.[155] (b) and (c) Probing of analyte biomolecules by analyte trigged self-assembly method using strongly coupled nanoparticles[30] (b) and nanorods[31] (c). Reprinted with permission from Copyright 2013 American Chemical Society, Copyright 2013 Nature Publishing Group.

In general, even a dense chiral molecule solution can only provide $\sim$ 10 millidegree of CD response, while that of the plasmonic structure can exceed $\sim$ 10 degrees. This is because the absorption and scattering cross-section of the latter are much larger than those of the former.[151] Therefore, a smart scheme has been developed to realize ultrasensitive chiral sensing: the analyte chiral molecules trigger the self-assembly of the plasmonic elements in solution, forming strongly coupled plasmonic structures that exhibit a much stronger CD signal. For instance, Wu *et al*. developed a heterodimer consisting of a large Au and a small Ag nanoparticle bridged by analyte biomolecules, to form a scissor-like geometry with a slightly twisted dimer axis.[30] The linked biomolecule can then be detected by measuring the large CD response of the dimer system (Fig. 11(b)). Using this method, it was determined that the LOD of the microcystin-LR and prostate-specific antigen can reach 10^{-13} M and 10^{-20} M, respectively. In a similar manner, Zhao *et al*. fabricated a shell-engineered heterodimer linked by DNA, and demonstrated the zeptomolar DNA detection.[159] By developing immunorecognition driven nanoparticle assembly, Xu *et al*. realized the probing of bisphenol-A with a LOD reaching 0.02 ng·mL^{-1}.[160] This self-assembly method can also be used to detect Ag ion with a concentration as low as 2 pM.[161] The preceding detection principles are all based on the non-ideal spherical shape or random defects of the nanoparticles that result in the low symmetry of the plasmonic geometries. To achieve a higher sensitivity, the symmetry of

the analyte linked plasmonic structures should be further reduced. As shown in Fig. 11(c), Ma *et al*. designed a side-by-side assembled nanorod chain with a small degree twist between the nanorod axes.[31] Based on the low symmetry of this system, they were able to achieve DNA detection down to 3.7 aM, where the CD signal exhibited a nearly linear relationship with the amount of target DNA. Chiral plasmonic molecules are also sensitive to their surrounding charge environment. This property has been utilized by Sun *et al*. to continuously monitor the transmembrane transport events of chiral dimers.[162] When the dimers travel from interstitial fluid to cytosol, the large change in electrostatic repulsion between the nanoparticles leads to the chirality reversal.

5.2. Nanoparticle growth and active plasmonic materials

Changes in the size and shape of plasmonic structures can also strongly modify their LSPR response, which in turn can be used as the basis for the development of plasmonic sensors to detect the physical, chemical and biological processes that induce the morphologic change of the plasmonic structures. A widely used method associated with nanoparticle enlargement for sensing biomolecules is bio-catalyzed reactions. In this scheme, the analyte behaves as a reducing agent to promote the growth of the nanoparticles situated in the solution, thereby resulting in a significant spectral change. Zayats *et al*. reported on the H_2O_2-mediated growth of Au nanoparticles that demonstrated the potential of this scheme for glucose sensing.[32] The H_2O_2 was produced from glucose by the catalysis of a glucose oxidase (GOx) and was used to reduce the Au ions into gold atoms in solution. This enzyme catalyzed assay has also been applied to the probing of a cancer biomarker prostate-specific antigen, with a LOD of 4×10^{-20} M in whole serum,[163] as demonstrated by Rodríguez-Lorenzo *et al*. They also found an inverse proportional relationship between the analyte concentration and the spectral variations. Liu *et al*. fabricated a GOx-catalyzed growth of 5-nm Au nanoparticles to detect prostate-specific antigens with a LOD as low as 93 aM. They demonstrated that this attomolar levels sensitivity is 4 orders of magnitude better than that obtained by commercial enzyme-linked immunosorbent assay.[164] In addition to the enlargement of the nanoparticles, the biocatalysis reaction can also lead to spectral changes caused by shape variation, *e.g.*, the transition of the Ag nanoparticle from nanoprisms to nanodisk geometry.[165] Although the use of GOx is predominant in this method, other enzymes such as hydrolytic proteins, hydroxylases and glucose dehydrogenase have been used in biocatalyst reactions to change the size of the nanoparticles.[92] Enzyme-mediated glucose sensors can also be applied to selectively kill cancer cells without harming normal cells.[166] This strategy is based on enzymatic H_2O_2 etching of GOx-modified Ag/Au nanoshells in the presence of glucose. Since the uptake rate of glucose in cancer cells is generally higher than for normal cells, the LSPR peak of the Ag/Au nanoshells situated around the cancer cells will red-shift to trigger higher photothermal effects when excited by a laser, resulting in the selective killing of the cancer cells.

The transformation between the metallic and dielectric properties of a nanomaterial can be viewed as an equivalent dimensional change of the LSPR-active structures. For example, metallic magnesium nanoparticles can be transformed into dielectric MgH_2 particles, resulting in the disappearance of the plasmonic response. Furthermore, the MgH_2 can be converted back into Mg in the presence of oxygen. The media involved in these switching processes are known as active plasmonic materials.[33] Duan *et al*. fabricated hybrid plasmonic nanostructures composed of Mg and Au nanoparticles with geometries that depict strong chiral optical response.[167] Upon hydrogen loading with increasing concentration, the CD response of the mixed structure gradually decreased due to the change of the plasmonic response via the conversion of Mg into MgH_2, and the reverse process occurred during the loading of oxygen. This study shows the potential for the development of active plasmonic platforms for a variety of gas detection schemes. Furthermore, the active plasmonic features of Mg have been extended for display applications.[168,169] An Mg nanolayer over an Al mirror separated by hydrogen silsesquioxane pillars of different heights can act as individual display pixels, whereby the color depends on the concentration of hydrogen loading. Apart from the Mg and MgH_2, similar processes can also work in the case of Ag and AgCl by electrochemical means, as demonstrated by Byers *et al*.[170] In their study, the Ag or AgCl served as the shell on the surface of the Au nanoparticle dimer, and the transition from the metallic Ag to dielectric AgCl leads to a spectral shift of a bonding plasmon and the emergence of a charge transfer plasmon due to the change in the effective gap distance. Therefore, Ag-based plasmonic structures also manifest the potential for probing various processes that can trigger the transition between metal and dielectric states.

5.3. Cavity optomechanics

With a built-in readout of the nanomechanical oscillator's motion displacement by analyzing the transmitted and reflected light from the cavity, cavity optomechanics[171] has developed into an important field for precise sensing of displacement (motion),[172–175] force,[176–179] and mass,[180–183] *etc*. However, the exploitation of the optomechanical coupling strength, which is highly related to the overall sensitivity, is unable to achieve the minimization requirements of the nanomechanical resonators due to the diffraction limit of light. The confinement of a conventional optical mode in a cavity is

approximately $\sim \lambda^3$, which is far from matching the volume of the nanoresonator. Recently, plasmonic nanocavities were introduced as a substitute for conventional microcavities in optomechanical measurement by virtue of their high sensitivity and breakthrough of the diffraction limit.[34,184,185] As indicated in previous sections, the LSPR in a nanocavity is highly sensitive to the surrounding medium's RI or to the physical to geometrical changes of the cavity. In addition, the near-field confined LSPR and free-space light can be easily interfaced in plasmonic antennas. This effect offers an opportunity for light to couple efficiently into or out of the optomechanical sensors. The light leaked from the sensor will contain the oscillation information of the nanomechanical element, which is collected and analyzed in the experiments.

As shown in Fig. 12(a), an experiment was performed by Thijssen *et al*. who introduced two parallel free-standing Au layer coated Si_3N_4 beams separated by 25 nm, and suspended on an Si_3N_4 membrane.[184] A coupled LSPR supported in the gap area was proposed to probe the thermal vibration of the nanomechanical beams at a frequency of 4.4 MHz. The vibration was transduced to a frequency dependent displacement function in terms of the intensity changes of the far-field transmission beam. Based on this configuration, they experimentally demonstrated that an enormous coupling constant G larger than 2 THz/nm could be achieved, and the displacement spectral density was measured as 1.11×10^{-13} m/Hz$^{1/2}$. Two years later, the group further integrated the coupling of a dipole–dipole nanorod dimer onto a pair of silicon nitride nanobeams[186] (Fig. 12(b)). In their experiment, the thermally driven mechanical motion of the nanobeams was converted to the shift of the dimer's LSPR, as reported by the intensity variation of the probe beam. As a result, the motion was measured with an imprecision spectral density of 207 fm/Hz$^{1/2}$, which approached the thermal limit of force sensitivity of 709 aN/Hz$^{1/2}$. A similar concept was adopted in a tunable suspended optical nanocavity which could be utilized in optomechanical systems.[185] Further work on LSPR-based optomechanical sensing has been realized by Roxworthy *et al*., who fabricated a nanoparticle planted cantilever that oscillated up and down over a metal pad,[34] as shown in Fig. 12(c). By applying a similar ratiometric transducer scheme to represent the cavity oscillation, a coupling G of 2 THz/nm was proposed for this nanopad-on-mirror system with a sensitive transduction of the mechanical motion and a noise floor of 6 fm/Hz$^{1/2}$.

However, with the development of optomechanics, the combination of LSPR and optomechanical nano-oscillators is encumbered by two major problems. The first problem is that compared with traditional dielectric microcavities, plasmonic nanocavities have a significantly lower Q-factor due to the inherent properties of plasmonic materials. Plasmo-mechanical systems may be more widely used for precise measurement and sensing only if this disadvantage can be effectively addressed. The second problem is the imprecision which arises from the weak and continuous measurement of two quadratures simultaneously: namely the position and the momentum. The conventional weak measurement is limited by the quantum mechanical Heisenberg uncertainty principle, especially for measurements where the precision is close to the zero-point fluctuation. In order to make meaningful progress towards breaking through this limit, single-quadrature measurement should be performed in order to measure one quadrature to an arbitrary precision.[187,188] Backaction evading measurement,[175,188,189] which has been realized in conventional optomechanical systems should be performed and reproduced in plasmo-mechanical systems to circumvent the limitation imposed by the uncertainty principle.

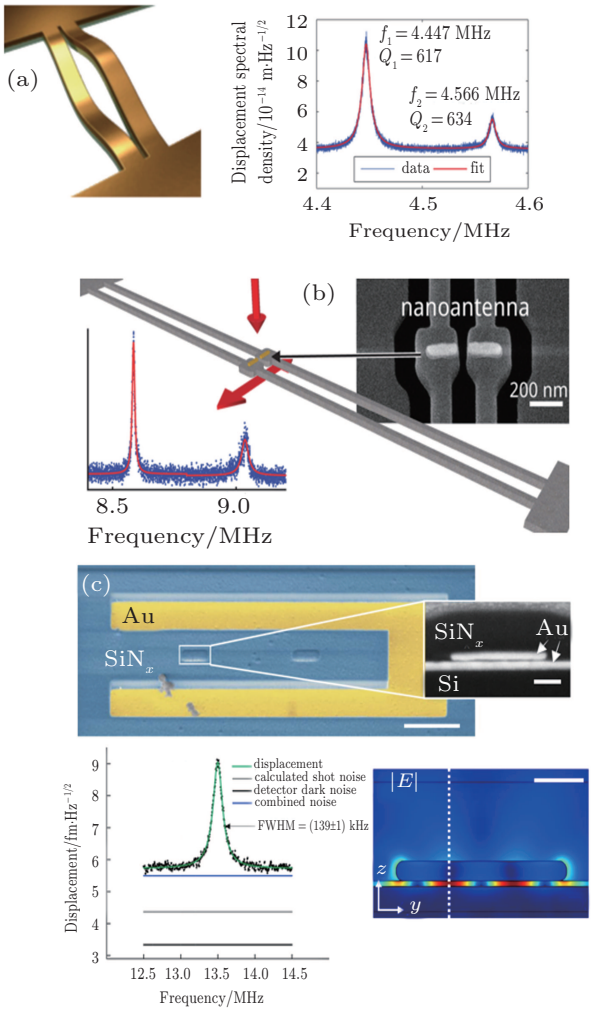


Fig. 12. (color online) LSPR-based cavity optomechanics. (a) Plasmon nanomechanical coupling of nanoscale separated beams.[184] (b) Plasmo-mechanical resonators based on dimer nano-antennas.[186] (c) Nanomechanical motion transduction with high order cavity plasmons.[34] Reprinted with permission from Copyright 2013, 2015 American Chemical Society, Copyright 2016 Nature Publishing Group.

6. Summary

In this review, we discussed some of the most important and promising research findings associated with LSPR-based

sensing, especially the individual plasmonic structures with spatial resolutions down to the nanoscale. The operation of the most of these sensors can be generally summarized as the effect of analytes or their relevant events that trigger spectral changes of the LSPR in plasmonic structures. They are detected via minute variations of their surrounding RI (refractometric sensing), displacement (plasmon ruler and plasmomechanical) or geometry (chiral sensing, active plasmonics and bio-catalysis, *etc*.). The resulting sensor output is then effectively read using far-field optics and is associated with corresponding changes in wavelength, intensity, phase, *etc*. Based on these principles, the LOD of an LSPR sensor mainly depends on the FOM of the plasmonic structure, as well as the spectral resolution of the measurement system. On one hand, the FOM is strongly related to the level of light confinement and sensing volume of the plasmon mode. The progress of the FOM associated with the choice of plasmon modes, generally developed from radiating bonding of plasmons to Fano resonances, and finally to cavity plasmons that manifest the potential of achieving the ultimate limit of the LSPR sensing sensitivity. On the other hand, a higher spectral resolution with a faster collection time is actively being pursued to realize real-time single-molecule detection with smaller molecular mass. These requirements are also desirable for precise monitoring of displacement with the goal of sub-picometer level detection using static plasmon rulers as well as oscillatory optomechanical transducers. In the future, the development of LSPR-based nanosensors will likely be divided into two main categories: one is to achieve low-cost, high-throughput and on-chip biosensing using simpler sample fabrication procedures, with the goal of single-molecule sensitivity for even smaller masses and higher selectivity, achieved by cheap and portable instruments. Another direction is the creation of a plasmonic nanocavity that facilitates the monitoring of ultrasmall cavity separation changes over ever smaller length scales. This could in principle be used for *in-situ* probing of very weak physical or chemical processes in atomic-thickness scale materials, *e.g.*, photoinduced stress, piezoelectric effects, optomechanics, atomic intercalation, and thermostriction, where the vertical dimensional changes need to be tracked with unprecedented accuracy and detail.

References

[1] Moskovits M 1985 *Rev. Mod. Phys.* **57** 783
[2] Fleischmann M, Hendra P J and McQuillan A J 1974 *Chem. Phys. Lett.* **26** 163
[3] Jeanmaire D L and Van Duyne R P 1977 *J. Electroanal. Chem.* **84** 1
[4] Kneipp K, Wang Y, Kneipp H, Perelman L T, Itzkan I, Dasari R and Feld M S 1997 *Phys. Rev. Lett.* **78** 1667
[5] Xu H X, Aizpurua J, Kall M and Apell P 2000 *Phys. Rev. E* **62** 4318
[6] Xu H X, Bjerneld E J, Käll M and Borjesson L 1999 *Phys. Rev. Lett.* **83** 4357
[7] Mayer K M, Hao F, Lee S, Nordlander P and Hafner J H 2010 *Nanotechnology* **21** 255503
[8] Ament I, Prasad J, Henkel A, Schmachtel S and Sonnichsen C 2012 *Nano Lett.* **12** 1092
[9] Zijlstra P, Paulo P M and Orrit M 2012 *Nat. Nanotech.* **7** 379
[10] Moerner W E 1999 *Science* **283** 1670
[11] Gaiduk A, Yorulmaz M, Ruijgrok P V and Orrit M 2010 *Science* **330** 353
[12] Chen S, Svedendahl M, Duyne R P and Kall M 2011 *Nano Lett.* **11** 1826
[13] Brolo A G 2012 *Nat. Photon.* **6** 709
[14] Svedendahl M, Chen S, Dmitriev A and Kall M 2009 *Nano Lett.* **9** 4428
[15] Homola J 2008 *Chem. Rev.* **108** 462
[16] Sherry L J, Chang S H, Schatz G C, Van Duyne R P, Wiley B J and Xia Y 2005 *Nano Lett.* **5** 2034
[17] Hao F, Sonnefraud Y, Dorpe P V, Maier S A, Halas N J and Nordlander P 2008 *Nano Lett.* **8** 3983
[18] Mirin N A, Bao K and Nordlander P 2009 *J. Phys. Chem. A* **113** 4028
[19] Liu N, Weiss T, Mesch M, Langguth L, Eigenthaler U, Hirscher M, Sonnichsen C and Giessen H 2010 *Nano Lett.* **10** 1103
[20] Lassiter J B, Sobhani H, Fan J A, Kundu J, Capasso F, Nordlander P and Halas N J 2010 *Nano Lett.* **10** 3184
[21] Liu N, Mesch M, Weiss T, Hentschel M and Giessen H 2010 *Nano Lett.* **10** 2342
[22] Verellen N, Van Dorpe P, Huang C, Lodewijks K, Vandenbosch G A, Lagae L and Moshchalkov V V 2011 *Nano Lett.* **11** 391
[23] Zhang S, Bao K, Halas N J, Xu H and Nordlander P 2011 *Nano Lett.* **11** 1657
[24] Pryce I M, Kelaita Y A, Aydin K and Atwater H A 2011 *ACS nano* **5** 8167
[25] Lopez-Tejeira F, Paniagua-Dominguez R and Sanchez-Gil J A 2012 *ACS Nano* **6** 8989
[26] Zhang S, Chen L, Huang Y and Xu H 2013 *Nanoscale* **5** 6985
[27] Esteban R, Aguirregabiria G, Borisov A G, Wang Y M, Nordlander P, Bryant G W and Aizpurua J 2015 *ACS Photon.* **2** 295
[28] Zhang S and Xu H 2016 *Nanoscale* **8** 13722
[29] Zhang H and Govorov A O 2013 *Phys. Rev. B* **87** 075410
[30] Wu X, Xu L, Liu L, Ma W, Yin H, Kuang H, Wang L, Xu C and Kotov N A 2013 *J. Am. Chem. Soc.* **135** 18629
[31] Ma W, Kuang H, Xu L, Ding L, Xu C, Wang L and Kotov N A 2013 *Nat. Commun.* **4** 2689
[32] Zayats M, Baron R, Popov I and Willner I 2005 *Nano Lett.* **5** 21
[33] Sterl F, Strohfeldt N, Walter R, Griessen R, Tittl A and Giessen H 2015 *Nano Lett.* **15** 7949
[34] Roxworthy B J and Aksyuk V A 2016 *Nat. Commun.* **7** 13746
[35] Maier S S A 2007 *Plasmonics: fundamentals and applications* (Springer Sciences & Business Media)
[36] Kreibig U and Vollmer M 2013 *Optical properties of metal clusters* (Springer Sciences & Business Media)
[37] Koppens F H L, Chang D E and García de Abajo F J 2011 *Nano Lett.* **11** 3370
[38] Grigorenko A N, Polini M and Novoselov K S 2012 *Nat. Photon.* **6** 749
[39] Xiang Y, Dai X, Guo J, Zhang H, Wen S and Tang D 2014 *Scientific Reports* **4** 5483
[40] Faucheaux J A, Stanton A L and Jain P K 2014 *J. Phys. Chem. Lett.* **5** 976
[41] Underwood S and Mulvaney P 1994 *Langmuir* **10** 3427
[42] McFarland A D and Van Duyne R P 2003 *Nano Lett.* **3** 1057
[43] Malinsky M D, Kelly K L, Schatz G C and Van Duyne R P 2001 *J. Am. Chem. Soc.* **123** 1471
[44] Mock J J, Smith D R and Schultz S 2003 *Nano Lett.* **3** 485
[45] Sun Y and Xia Y 2002 *Anal. Chem.* **74** 5297
[46] Tam F, Moran C and Halas N 2004 *J. Phys. Chem. B* **108** 17290
[47] Raschke G, Brogl S, Susha A S, Rogach A L, Klar T A, Feldmann J, Fieres B, Petkov N, Bein T, Nichtl A and Kürzinger K 2004 *Nano Lett.* **4** 1853
[48] Wang H, Brandl D W, Le F, Nordlander P and Halas N J 2006 *Nano Lett.* **6** 827
[49] Nehl C L, Liao H and Hafner J H 2006 *Nano Lett.* **6** 683
[50] Bukasov R and Shumaker-Parry J S 2007 *Nano Lett.* **7** 1113
[51] Chen H, Kou X, Yang Z, Ni W and Wang J 2008 *Langmuir* **24** 5233
[52] Mayer K M, Lee S, Liao H, Rostro B C, Fuentes A, Scully P T, Nehl C L and Hafner J H 2008 *ACS Nano* **2** 687
[53] Burgin J, Liu M and Guyot-Sionnest P 2008 *J. Phys. Chem. C* **112** 19279

[54] Khalavka Y, Becker J and Sonnichsen C 2009 *J. Am. Chem. Soc.* **131** 1871
[55] Yanik A A, Cetin A E, Huang M, Artar A, Mousavi S H, Khanikaev A, Connor J H, Shvets G and Altug H 2011 *Proc. Natl. Acad. Sci.* **108** 11784
[56] Shen Y, Zhou J, Liu T, Tao Y, Jiang R, Liu M, Xiao G, Zhu J, Zhou Z K, Wang X, Jin C and Wang J 2013 *Nat. Commun.* **4** 2381
[57] Su K H, Wei Q H, Zhang X, Mock J J, Smith D R and Schultz S 2003 *Nano Lett.* **3** 1087
[58] Mayer K M and Hafner J H 2011 *Chem. Rev.* **111** 3828
[59] Raschke G, Kowarik S, Franzl T, Sönnichsen C, Klar T A, Feldmann J, Nichtl A and Kürzinger K 2003 *Nano Lett.* **3** 935
[60] Hao F, Nehl C L, Hafner J H and Nordlander P 2007 *Nano Lett.* **7** 729
[61] Gallinet B, Siegfried T, Sigg H, Nordlander P and Martin O J 2013 *Nano Lett.* **13** 497
[62] Miller M M and Lazarides A A 2005 *J. Phys. Chem. B* **109** 21556
[63] Tong L, Wei H, Zhang S and Xu H 2014 *Sensors* **14** 7959
[64] Auguié B and Barnes W L 2008 *Phys. Rev. Lett.* **101** 143902
[65] Kravets V, Schedin F and Grigorenko A 2008 *Phys. Rev. Lett.* **101** 087403
[66] Vecchi G, Giannini V and Gómez Rivas J 2009 *Phys. Rev. B* **80** 201401(R)
[67] Lu H, Liu X, Mao D and Wang G 2012 *Opt. Lett.* **37** 3780
[68] Chen J, Li Z, Zou Y, Deng Z, Xiao J and Gong Q 2013 *Plasmonics* **8** 1627
[69] Qi J, Chen Z, Chen J, Li Y, Qiang W, Xu J and Sun Q 2014 *Opt. Exp.* **22** 14688
[70] Lai G, Liang R, Zhang Y, Bian Z, Yi L, Zhan G and Zhao R 2015 *Opt. Exp.* **23** 6554
[71] Dahlin A B, Tegenfeldt J O and Hook F 2006 *Anal. Chem.* **78** 4416
[72] Thomsen V, Schatzlein D and Mercuro D 2003 *Spectroscopy* **18** 112
[73] Homola J and Piliarik M 2006 *Surface Plasmon Resonance (SPR) Sensors* (Springer) 45–67
[74] Lodewijks K, Van Roy W, Borghs G, Lagae L and Van Dorpe P 2012 *Nano Lett.* **12** 1655
[75] Homola J and Piliarik M 2006 *SPR Sensor Instrumentation* (Springer) 95–114
[76] Johansen K, Stölberg R, Lundström I and Liedberg B 2000 *Meas. Sci. Technol.* **11** 1630
[77] Nenninger G G, Piliarik M and Homola J 2002 *Meas. Sci. Technol.* **13** 2038
[78] Thirstrup C and Zong W 2005 *Sens. Actuators B: Chem.* **106** 796
[79] Zhan S, Wang X and Liu Y 2011 *Meas. Sci. Technol.* **22** 025201
[80] Sjoelander S and Urbaniczky C 1991 *Anal. Chem.* **63** 2338
[81] Stenberg E, Persson B, Roos H and Urbaniczky C 1991 *J. Colloid Interface Sci.* **143** 513
[82] Chinowsky T M, Jung L S and Yee S S 1999 *Sens. Actuators B: Chem.* **54** 89
[83] Abumazwed A, Kubo W, Shen C, Tanaka T and Kirk A G 2017 *Biomed. Opt. Exp.* **8** 446
[84] Das M, Hohertz D, Nirwan R, Brolo A G, Kavanagh K L and Gordon R 2011 *IEEE Photonics Journal* **3** 441
[85] Chen P and Liedberg B 2014 *Anal. Chem.* **86** 7399
[86] Chen P, Tran N T, Wen X, Xiong Q and Liedberg B 2017 *ACS sensors* **2** 235
[87] Chen S, Svedendahl M, Kall M, Gunnarsson L and Dmitriev A 2009 *Nanotechnology* **20** 434015
[88] Anker J N, Hall W P, Lyandres O, Shah N C, Zhao J and Van Duyne R P 2008 *Nat. Mater.* **7** 442
[89] Unser S, Bruzas I, He J and Sagle L 2015 *Sensors* **15** 15684
[90] Whitney A V, Elam J W, Zou S, Zinovev A V, Stair P C, Schatz G C and Van Duyne R P 2005 *J. Phys. Chem. B* **109** 20522
[91] Spackova B, Wrobel P, Bockova M and Homola J 2016 *Proc. IEEE* **104** 2380
[92] Guo L, Jackman J A, Yang H H, Chen P, Cho N J and Kim D H 2015 *Nano Today* **10** 213
[93] Haes A J, Chang L, Klein W L and Van Duyne R P 2005 *J. Am. Chem. Soc.* **127** 2264
[94] Guo L and Kim D H 2012 *Biosens. Bioelectron.* **31** 567
[95] Bingham J M, Anker J N, Kreno L E and Van Duyne R P 2010 *J. Am. Chem. Soc.* **132** 17358
[96] Haes A J, Zou S, Zhao J, Schatz G C and Van Duyne R P 2006 *J. Am. Chem. Soc.* **128** 10905
[97] Zhao J, Das A, Zhang X, Schatz G C, Sligar S G and Van Duyne R P 2006 *J. Am. Chem. Soc.* **128** 11004
[98] Zhao J, Jensen L, Sung J, Zou S, Schatz G C and Duyne R P 2007 *J. Am. Chem. Soc.* **129** 7647
[99] Haes A J, Stuart D A, Nie S and Van Duyne R P 2004 *J. Fluoresc.* **14** 355
[100] Larsson E M, Alegret J, Käll M and Sutherland D S 2007 *Nano Lett.* **7** 1256
[101] Nusz G J, Curry A C, Marinakos S M, Wax A and Chilkoti A 2009 *ACS Nano* **3** 795
[102] Halas N J, Lal S, Chang W S, Link S and Nordlander P 2011 *Chem. Rev.* **111** 3913
[103] Elghanian R, Storhoff J J, Mucic R C, Letsinger R L and Mirkin C A 1997 *Science* **277** 1078
[104] Saha K, Agasti S S, Kim C, Li X and Rotello V M 2012 *Chem. Rev.* **112** 2739
[105] Sonnichsen C, Reinhard B M, Liphardt J and Alivisatos A P 2005 *Nat. Biotech.* **23** 741
[106] Gunnarsson L, Rindzevicius T, Prikulis J, Kasemo B, Kall M, Zou S and Schatz G C 2005 *J. Phys. Chem. B* **109** 1079
[107] Jain P K, Huang W and El-Sayed M A 2007 *Nano Lett.* **7** 2080
[108] Reinhard B M, Siu M, Agarwal H, Alivisatos A P and Liphardt J 2005 *Nano Lett.* **5** 2246
[109] Funston A M, Novo C, Davis T J and Mulvaney P 2009 *Nano Lett.* **9** 1651
[110] Huang C P, Yin X G, Kong L B and Zhu Y Y 2010 *J. Phys. Chem. C* **114** 21123
[111] Bordley J A, Hooshmand N and El-Sayed M A 2015 *Nano Lett.* **15** 3391
[112] Jain P K and El-Sayed M A 2007 *Nano Lett.* **7** 2854
[113] Kadkhodazadeh S, de Lasson J R, Beleggia M, Kneipp H, Wagner J B and Kneipp K 2014 *J. Phys. Chem. C* **118** 5478
[114] Dolinnyi A I 2015 *J. Phys. Chem. C* **119** 4990
[115] Hill R T, Mock J J, Hucknall A, Wolter S D, Jokerst N M, Smith D R and Chilkoti A 2012 *ACS Nano* **6** 9237
[116] Prodan E, Radloff C, Halas N J and Nordlander P 2003 *Science* **302** 419
[117] Nordlander P, Oubre C, Prodan E, Li K and Stockman M I 2004 *Nano Lett.* **4** 899
[118] Nordlander P and Prodan E 2004 *Nano Lett.* **4** 2209
[119] Rechberger W, Hohenau A, Leitner A, Krenn J R, Lamprecht B and Aussenegg F R 2003 *Opt. Commun.* **220** 137
[120] Lassiter J B, McGuire F, Mock J J, Ciraci C, Hill R T, Wiley B J, Chilkoti A and Smith D R 2013 *Nano Lett.* **13** 5866
[121] Chen W, Zhang S, Deng Q and Xu H 2018 *Nat. Commun.* **9** 801
[122] Esteban R, Borisov A G, Nordlander P and Aizpurua J 2012 *Nat. Commun.* **3** 825
[123] Ciraci C, Hill R T, Mock J J, Urzhumov Y, Fernandez-Dominguez A I, Maier S A, Pendry J B, Chilkoti A and Smith D R 2012 *Science* **337** 1072
[124] Savage K J, Hawkeye M M, Esteban R, Borisov A G, Aizpurua J and Baumberg J J 2012 *Nature* **491** 574
[125] Zhu W, Esteban R, Borisov A G, Baumberg J J, Nordlander P, Lezec H J, Aizpurua J and Crozier K B 2016 *Nat. Commun.* **7** 11495
[126] Tan S F, Wu L, Yang J K, Bai P, Bosman M and Nijhuis C A 2014 *Science* **343** 1496
[127] Lerch S and Reinhard B M 2016 *Adv. Mater.* **28** 2030
[128] Hentschel M, Saliba M, Vogelgesang R, Giessen H, Alivisatos A P and Liu N 2010 *Nano Lett.* **10** 2721
[129] Shao L, Fang C, Chen H, Man Y C, Wang J and Lin H Q 2012 *Nano Lett.* **12** 1424
[130] Liu N, Hentschel M, Weiss T, Alivisatos A P and Giessen H 2011 *Science* **332** 1407
[131] Ray P C, Fan Z, Crouch R A, Sinha S S and Pramanik A 2014 *Chem. Soc. Rev.* **43** 6370
[132] Morimura H, Tanaka S, Ishitobi H, Mikami T, Kamachi Y, Kondoh H and Inouye Y 2013 *ACS Nano* **7** 10733
[133] Reinhard B M, Sheikholeslami S, Mastroianni A, Alivisatos A P and Liphardt J 2007 *Proc. Natl. Acad. Sci.* **104** 2667
[134] Chen T, Hong Y and Reinhard B M 2015 *Nano Lett.* **15** 5349

[135] Qian G S, Zhang T T, Zhao W, Xu J J and Chen H Y 2017 *Chem. Commun.* **53** 4710
[136] Skewis L R and Reinhard B M 2008 *Nano Lett.* **8** 214
[137] Chen J I, Chen Y and Ginger D S 2010 *J. Am. Chem. Soc.* **132** 9600
[138] Chen J I, Durkee H, Traxler B and Ginger D S 2011 *Small* **7** 1993
[139] Lermusiaux L and Bidault S 2015 *Small* **11** 5696
[140] Guo L, Ferhan A R, Chen H, Li C, Chen G, Hong S and Kim D H 2013 *Small* **9** 234
[141] Lee S E, Chen Q, Bhat R, Petkiewicz S, Smith J M, Ferry V E, Correia A L, Alivisatos A P and Bissell M J 2015 *Nano Lett.* **15** 4564
[142] Rong G, Wang H, Skewis L R and Reinhard B M 2008 *Nano Lett.* **8** 3386
[143] Rong G, Wang H and Reinhard B M 2010 *Nano Lett.* **10** 230
[144] Jun Y W, Sheikholeslami S, Hostetter D R, Tajon C, Craik C S and Alivisatos A P 2009 *Proc. Natl. Acad. Sci.* **106** 17735
[145] Tajon C A, Seo D, Asmussen J, Shah N, Jun Y W and Craik C S 2014 *ACS Nano* **8** 9199
[146] Ding T, Rüttiger C, Zheng X, Benz F, Ohadi H, Vandenbosch G A E, Moshchalkov V V, Gallei M and Baumberg J J 2016 *Adv. Opt. Mater.* **4** 877
[147] Powell A W, Coles D M, Taylor R A, Watt A A R, Assender H E and Smith J M 2016 *Adv. Opt. Mater.* **4** 634
[148] Cataldi U, Caputo R, Kurylyak Y, Klein G, Chekini M, Umeton C and Bürgi T 2014 *J. Mater. Chem. C* **2** 7927
[149] Maurer T, Marae-Djouda J, Cataldi U, *et al.* 2015 *Front. Mater. Sci.* **9** 170
[150] Berova N, Nakanishi K and Woody R 2000 *Circular dichroism: principles and applications* (John Wiley & Sons)
[151] Hentschel M, Schaferling M, Duan X, Giessen H and Liu N 2017 *Sci. Adv.* **3** e1602735
[152] Govorov A O, Gun'ko Y K, Slocik J M, Gerard V A, Fan Z and Naik R R 2011 *J. Mater. Chem.* **21** 16806
[153] Ben-Moshe A, Maoz B M, Govorov A O and Markovich G 2013 *Chem. Soc. Rev.* **42** 7028
[154] Maoz B M, Chaikin Y, Tesler A B, Bar Elli O, Fan Z, Govorov A O and Markovich G 2013 *Nano Lett.* **13** 1203
[155] Lu F, Tian Y, Liu M, Su D, Zhang H, Govorov A O and Gang O 2013 *Nano Lett.* **13** 3145
[156] Wang H, Li Z, Zhang H, Wang P and Wen S 2015 *Scientific Reports* **5** 8207
[157] Schäferling M, Yin X, Engheta N and Giessen H 2014 *ACS Photon.* **1** 530
[158] Hendry E, Carpy T, Johnston J, Popland M, Mikhaylovskiy R V, Lapthorn A J, Kelly S M, Barron L D, Gadegaard N and Kadodwala M 2010 *Nat. Nanotech.* **5** 783
[159] Zhao Y, Xu L, Ma W, Wang L, Kuang H, Xu C and Kotov N A 2014 *Nano Lett.* **14** 3908
[160] Xu Z, Xu L, Zhu Y, Ma W, Kuang H, Wang L and Xu C 2012 *Chem. Commun.* **48** 5760
[161] Xu Z, Xu L, Liz-Marzán L M, Ma W, Kotov N A, Wang L, Kuang H and Xu C 2013 *Adv. Opt. Mater.* **1** 626
[162] Sun M, Xu L, Banhg J H, Kuang H, Alben S, Kotov N A and Xu C 2017 *Nat. Commun.* **8** 1847
[163] Rodriguez-Lorenzo L, de la Rica R, Alvarez-Puebla R A, Liz-Marzan L M and Stevens M M 2012 *Nat. Mater.* **11** 604
[164] Liu D, Yang J, Wang H F, Wang Z, Huang X, Wang Z, Niu G, Hight Walker A R and Chen X 2014 *Anal. Chem.* **86** 5800
[165] Xia Y, Ye J, Tan K, Wang J and Yang G 2013 *Anal. Chem.* **85** 6241
[166] Chen L, Li H, He H, Wu H and Jin Y 2015 *Anal. Chem.* **87** 6868
[167] Duan X, Kamin S, Sterl F, Giessen H and Liu N 2016 *Nano Lett.* **16** 1462
[168] Chen Y, Duan X, Matuschek M, Zhou Y, Neubrech F, Duan H and Liu N 2017 *Nano Lett.* **17** 5555
[169] Duan X, Kamin S and Liu N 2017 *Nat. Commun.* **8** 14606
[170] Byers C P, Zhang H, Swearer D F, Yorulmaz M, Hoener B S, Huang D, Hoggard A, Chang W S, Mulvaney P, Ringe E, Halas N J, Nordlander P, Link S and Landes C F 2015 *Sci. Adv.* **1** e1500988
[171] Aspelmeyer M, Kippenberg T J and Marquard F 2014 *Rev. Mod. Phys.* **86** 1391
[172] Arcizet O, Cohadon P F, Briant T, Pinard M, Heidmann A, Mackowski J M, Michel C, Pinard L, Francais O and Rousseau L 2006 *Phys. Rev. Lett.* **97** 133601
[173] Teufel J D, Donner T, Castellanos-Beltran M A, Harlow J W and Lehnert K W 2009 *Nat. Nanotech.* **4** 820
[174] Anetsberger G, Arcizet O, Unterreithmeier Q P, Riviere R, Schliesser A, Weig E M, Kotthaus J P and Kippenberg T J 2009 *Nat.Phys.* **5** 909
[175] Hertzberg J B, Rocheleau T, Ndukum T, Savva M, Clerk A A and Schwab K C 2009 *Nat.Phys.* **6** 213
[176] Mamin H J and Rugar D 2001 *Appl. Phys. Lett.* **79** 3358
[177] Gavartin E, Verlot P and Kippenberg T J 2012 *Nat. Nanotech.* **7** 509
[178] Hempston D, Vovrosh J, Toroš M, Winstone G, Rashid M and Ulbricht H 2017 *Appl. Phys. Lett.* **111** 133111
[179] Zhang W Z, Han Y, Xiong B and Zhou L 2017 *New J. Phys.* **19** 083022
[180] Ekinci K L, Yang Y T and Roukes M L 2004 *J. Appl. Phys.* **95** 2682
[181] Jensen K, Kim K and Zettl A 2008 *Nat. Nanotech.* **3** 533
[182] Tamayo J 2015 *Nat. Nanotech.* **10** 738
[183] He Y 2015 *Appl. Phys. Lett.* **106** 121905
[184] Thijssen R, Verhagen E, Kippenberg T J and Polman A 2013 *Nano Lett.* **13** 3293
[185] Chen K, Razinskas G, Feichtner T, Grossmann S, Christiansen S and Hecht B 2016 *Nano Lett.* **16** 2680
[186] Thijssen R, Kippenberg T J, Polman A and Verhagen E 2015 *Nano Lett.* **15** 3971
[187] Caves C M, Thorne K S, Drever R W P, Sandberg V D and Zimmermann M 1980 *Rev. Mod. Phys.* **52** 341
[188] Clerk A A, Marquardt F and Jacobs K 2008 *New J. Phys.* **10** 095010
[189] Moller C B, Thomas R A, Vasilakis G, Zeuthen E, Tsaturyan Y, Balabas M, Jensen K, Schliesser A, Hammerer K and Polzik E S 2017 *Nature* **547** 191